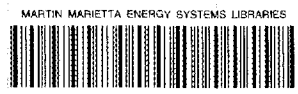

ORNL/TM-9821

ornl

OAK RIDGE NATIONAL LABORATORY

MARTIN MARIETTA

Dynamic Behavior and Control Requirements of an Atmospheric Fluidized-Bed Coal Combustion Power Plant: A Conceptual Study

O. L. Smith

OPERATED BY
MARTIN MARIETTA ENERGY SYSTEMS, INC.
FOR THE UNITED STATES
DEPARTMENT OF ENERGY

Printed in the United States of America. Available from
National Technical Information Service
U.S. Department of Commerce
5285 Port Royal Road, Springfield, Virginia 22161
NTIS price codes—Printed Copy: A05 Microfiche A01

ORNL/TM-9821

Instrumentation and Controls Division

DYNAMIC BEHAVIOR AND CONTROL REQUIREMENTS OF AN ATMOSPHERIC FLUIDIZED-BED COAL COMBUSTION POWER PLANT: A CONCEPTUAL STUDY

O. L. Smith

Date of Issue: June 1987

Prepared by the
OAK RIDGE NATIONAL LABORATORY
Oak Ridge, Tennessee 37831
operated by
MARTIN MARIETTA ENERGY SYSTEMS, INC.
for the
U.S. DEPARTMENT OF ENERGY
under Contract No. DE-AC05-84OR21400

TABLE OF CONTENTS

LIST OF FIGURES v

LIST OF TABLES viii

ABSTRACT ix

1. INTRODUCTION 1

2. MATHEMATICAL DEVELOPMENT 7

2.1 WATER/STEAM CIRCUIT 7
2.1.1 Boiler 7
2.1.2 Primary Superheater 18
2.1.3 Secondary (Inbed) Superheater 19
2.1.4 Steam Drum 20
2.1.5 Attemperator 21
2.1.6 Air-cooled Condenser 22
2.1.7 Economizer 23

2.2 AIR AND GAS PATH 23
2.2.1 Air Preheater 23
2.2.2 Forced Draft Flow 24
2.2.3 Bed 25
2.2.4 Convection Zone 31
2.2.5 Induced Draft Flow 32

2.3 SUMMARY OF STATE VARIABLE EQUATIONS 33

3. PARAMETERS 34

4. OPEN-LOOP ANALYSIS 35

4.1 INHERENT DYNAMICS 35
4.1.1 Air Inlet Damper Setting 42
4.1.2 Effective Evaporator Heat Transfer Surface 43
4.1.3 Primary Superheater Transfer Surface 44
4.1.4 Secondary (Bed) Superheater Transfer Surface . . . 44

4.2 INFLUENCE OF FEEDWATER HEATING ON DYNAMICS 45

5. PLANT CONTROL 47

5.1 CONTROLLER DESIGN 47
5.2 CONTROLLER TUNING 49
5.3 TIME DELAYS IN A FLUID-BED PLANT 50
5.4 LOAD FOLLOWING 55
5.4.1 Abrupt Change 55
5.4.2 Ramp Change 56

ACKNOWLEDGMENT 71

REFERENCES 72

APPENDIX 73

LIST OF FIGURES

FIGURE		PAGE
1.	Model of a fluid-bed pilot plant	5
2a.	SO_2 in flue gas	30
2b.	Total elutriation as a function of superficial velocity	30
3a.	Open-loop response to 1% reduction of coal feed	39
3b.	Power generation in evaporator	39
3c.	Power generation in primary (above-bed) superheater	39
3d.	Power generation in secondary (in-bed) superheater	39
3e.	Bed temperature	40
3f.	Throttle steam temperature	40
3g.	Drum pressure (1) and throttle steam pressure (2)	40
4.	Control system	48
5.	Controlled response of drum (1) and throttle (2) pressures to 5% step reduction in load	51
6.	Divergent pressure response with gain increased twofold	51
7.	Controlled response of drum (1) and throttle (2) pressures to 5% step change in load with reset in coal-feed loop	51
8.	Reaction curve analysis of system time lags	53
9.	Effect of adding derivative action to coal-feed control	56
10a.	Effect on system variables of 5% step reduction in load	57
10b.	SO_2 capture	57
10c.	Limestone feed	57
10d.	Steam pressure	57
10e.	Coal feed	58

11a. Effect on system variables of 25% runback of load at rate of 0.75%/min, with bed slumping after runback 60

11b. Main steam flow 60

11c. Power generation 60

11d. Coal feed 60

11e. Superficial velocity 61

11f. Steam pressure 61

11g. Temperature 61

11h. SO_2 capture 61

11i. Limestone feed 62

11j. Control valve settings 62

11k. Fraction of bed fluidized and heat transfer surface active 62

12a. Effect on system variables of 25% runback of load at 0.75%/min, with variable bed height 64

12b. Main steam flow 64

12c. Power generation 64

12d. Coal feed 64

12e. Superficial velocity 65

12f. Steam pressure 65

12g. Temperature 65

12h. SO_2 capture 65

12i. Limestone feed 66

12j. Control valve settings 66

12k. Fraction of bed fluidized and heat transfer surface active 66

13a. Maximum load-following capability (5%/min) using variable bed heights 68

13b. Main steam flow 68

13c. Power generation 68

13d. Coal feed 68

13e. Superficial velocity 69

13f. Steam pressure 69

13g. Temperature 69

13h. SO_2 capture 69

13i. Limestone feed 70

13j. Control valve settings 70

13k. Fraction of bed fluidized and heat transfer surface active 70

LIST OF TABLES

TABLE		PAGE
1.	Symbols and values	8
2.	Nominal values of parameters and variables	36
3.	Sensitivity of AFBC state variables to changes in selected system parameters	37
4.	Some effects of adding feedwater heating	46
5.	Controller settings	49
6.	Principal system heat capacities expressed in full power minutes of stored heat	52

ABSTRACT

A first-principles model of a nominal 20-MW atmospheric-pressure fluidized-bed coal combustion (AFBC) power plant was developed to provide insight into fundamental dynamic behavior of fluidized-bed systems. Air preheater, steam drum, evaporator, primary and secondary superheater, induced and forced draft fans, economizer, attemperator, bed, coal and limestone supply systems, and air-cooled condenser were explicitly represented. The air-gas path was included from intake to stack exhaust, and the entire steam loop was treated except for dynamically minor parts such as the demineralization system. The control system included major loops for firing rate, steam pressure and temperature, forced and induced draft air flow, SO_2 emission, drum water level, evaporator recirculation, and bed level.

The model was used to investigate system sensitivity to design features such as the distribution of heat transfer surface among the bed boiler and superheater and the out-of-bed superheater. Also calculated were the sensitivities of temperatures, pressures, and flow rates to changes in throttle, attemperator, and feedwater valve settings and forced and induced draft damper settings.

The large bed mass, accounting for ~40% of the active heat capacity, may vary under load change and could impact controller tuning. Model analysis indicated, however, that for the design studied, the change in bed mass does not appear to significantly affect controller tuning even if the bed mass varies appreciably under load-following conditions.

Several bed designs are being considered for AFBC plants, some with partitions between bed sections and some without, and these differences may significantly affect the load-following capability of the plant. One design calls for complete shutdown (slumping) of individual sections of the bed as load decreases. Another design involves lowering the bed height uniformly across the bed to expose and deactivate submerged heat transfer tubes without shutting down bed sections. The model was used for comparative studies of the maximum rate of load change that a plant

could follow with the two designs. The second method showed significantly better control characteristics. The results indicated that the slumping mode of operation can cause distortion of the heat source/sink distribution in the bed such that the load-following capability (rate of load change) of the plant may be reduced by as much as a factor of 5 compared with the mode in which tube surface is exposed.

1. INTRODUCTION

A fluidized-bed power plant differs from a conventional pulverized coal plant in ways that may result in significant differences in the basic dynamics of the plant and control system. Early emphasis on these differences may aid in matching the control package to the plant's inherent behavior and reduce the likelihood of having to retrofit the controls later in the program. Design differences that may prove dynamically important include the following.

1. Bed temperature is about half that of a conventional plant. The lower temperature affects heat transfer, storage, and distribution among boiler components and thereby influences plant time constants and the rate and manner of response to load variation.

2. Bed temperature must be maintained within a limited range around 1550°F to hold SO_2 sorption to Environmental Protection Agency (EPA) requirements. This constraint may mean that other variables will be held to narrower tolerances than in a conventional plant, using refined instrumentation or a more rigorous control philosophy. If the plant is to have load-following flexibility, a suitable strategy will be needed to constrain the bed temperature even under strong load variation.

3. The heat transfer coefficient in the bed is fairly insensitive to changes in gas velocity. Variation of flow through the furnace appears not to be a useful control technique as it is in a conventional plant.

Bed slumping, in which whole segments are put into or removed from service, is a planned alternative means of load following. Since slumping has step-wise aspects, whereas load demand may be a relatively smooth ramp, there could be problems in matching load and firing rate over the full range. The magnitude of the difficulty would depend in part on the number of bed segments and the fraction of power associated with each. Compartment manipulations amount to system disturbances, and the dynamics will allow them to be accomplished only at a certain rate

without causing excessive pressure and temperature transients. The capability of a plant to automatically handle compartment shutdown and startup and to trim heat output between steps remains to be determined.

4. In a conventional plant, heat transfer surfaces are mainly outside the firebox, and the principal means of heat absorption is by radiation or convective transfer from hot gases. With heat absorption proportioned between boiler and superheaters for full load, the inherent behavior of the plant at load turndown is for the heat absorbed in the boiler to increase disproportionately and that absorbed in the superheater to decrease; the control system is tailored to this behavior pattern.

In an atmospheric-pressure fluidized-bed combustion (AFBC) plant, a major portion of the generated heat may be extracted at boiler and superheat surfaces immersed in the firebox, where conductive rather than radiative or convective heat transfer will be the principal absorption mechanism. These differences in design and thermohydrodynamics raise the question of whether the inherent load-following (or not following) tendency of a fluidized-bed combustor may differ in principle or magnitude from that of a conventional plant.

If distribution of heat extraction between bed boiler and superheater is to be controlled by turning down boiler compartments at a rate different from superheater compartments, it will have to be established that this procedure, with its step-wise aspects, affords sufficient flexibility to achieve the required range of heat distribution.

5. The large heat capacity of the bed, unique among coal plants, will contribute to plant dynamics and may affect controller design.

6. The fluidized-bed concept introduces a new method of sulphur removal, with new control requirements and problems.

System simulation may provide information on these and other factors that influence plant dynamics and the design of efficient controls. The work reported here has principal objectives of

a. developing a simplified yet realistic model of a plant to determine dynamic characteristics of the fluid bed that differ from those of conventional pulverized coal plants,
b. investigating types of control and instrumentation that can efficiently handle unique requirements of the fluid bed boiler, and
c. providing information on how the dynamic performance of the plant is affected by specific design parameters such as superficial velocity, distribution of heat between bed superheaters and boiler compartments, and between in-bed and above-bed heat transfer surface.

In any attempt to model a fluidized bed, the limited amount of currently available data needs to be taken into account: model complexity should be consistent with data detail since an overextended simulation cannot be properly tested. The level of detail in the present model should lend itself to suitable testing. A first-principles model[1] is an appropriate level of resolution for providing insight into fundamental system behavior. Such a model is structured from basic system components, and many conventional details that add to overall plant efficiency but have a modest effect on dynamics are omitted. Principal time constants and primary control requirements are emphasized, and sensitivity analyses show how plant performance is affected by possible ranges of major parameters.

In the present work, the plant model incorporates features that are fundamental to fluidized systems [e.g., boiler and superheater (SH) surfaces and a mass of limestone in the firebox] and which are important in determining generic dynamics. The model is readily modified. Additional details may be added to simulate the system at whatever level of sophistication appears warranted. The model parameters are set for a low-power facility but may be extended to higher-power systems.

There are four major sections of the model. The first calculates initial steady state flow rates, temperatures, pressures and other thermodynamic quantities for a given power level and system

parameters. The air preheater, steam drum, evaporator, primary and secondary superheater, induced draft (ID) and forced draft (FD) fans, economizer, attemperator, bed, coal and limestone supply systems, and air-cooled condenser are explicitly represented (Fig. 1). The air-gas path is represented from intake to stack exhaust, and the full steam loop is treated except for dynamically minor parts such as the demineralization system.

The second section of the model calculates transient response induced by changes in load, coal feed, valve settings, or other disturbances. Within the guideline of developing a simplified yet meaningful simulation, the number of differential equations was held to twelve. These represent the independent state variables of bed temperature, evaporator metal temperature, primary and secondary superheater metal temperature, preheater metal temperature, coal feed rate, coal burnup rate, density of steam and volume of water in the drum, gas density and temperature at the furnace outlet, and condenser metal temperature. The differential equations are supplemented by algebraic equations for pumps and other mechanical components and by experimental correlations (extracted primarily from standard steam tables) for the remaining system variables.

AFBC state variables often change slowly during a transient and take many minutes to reach new equilibria. The variations may be such that if the initial state, the beginning portion of the transient, and the final state are known, the remainder of the transient can be "roughed in" visually with accuracy sufficient to judge how fast and how much things change. To take advantage of this, the third section of the model is a subroutine that causes the code to skip to the final state at a preset time in the transient and compute new equilibrium conditions from a set of nonlinear coupled algebraic equations. Computer running time is typically reduced by two-thirds with this speedup device and is particularly economical when parametric studies are run.

The first and third sections (initial and final conditions) are used jointly in a sensitivity analysis to determine how a change or uncertainty in one variable or parameter affects the others.

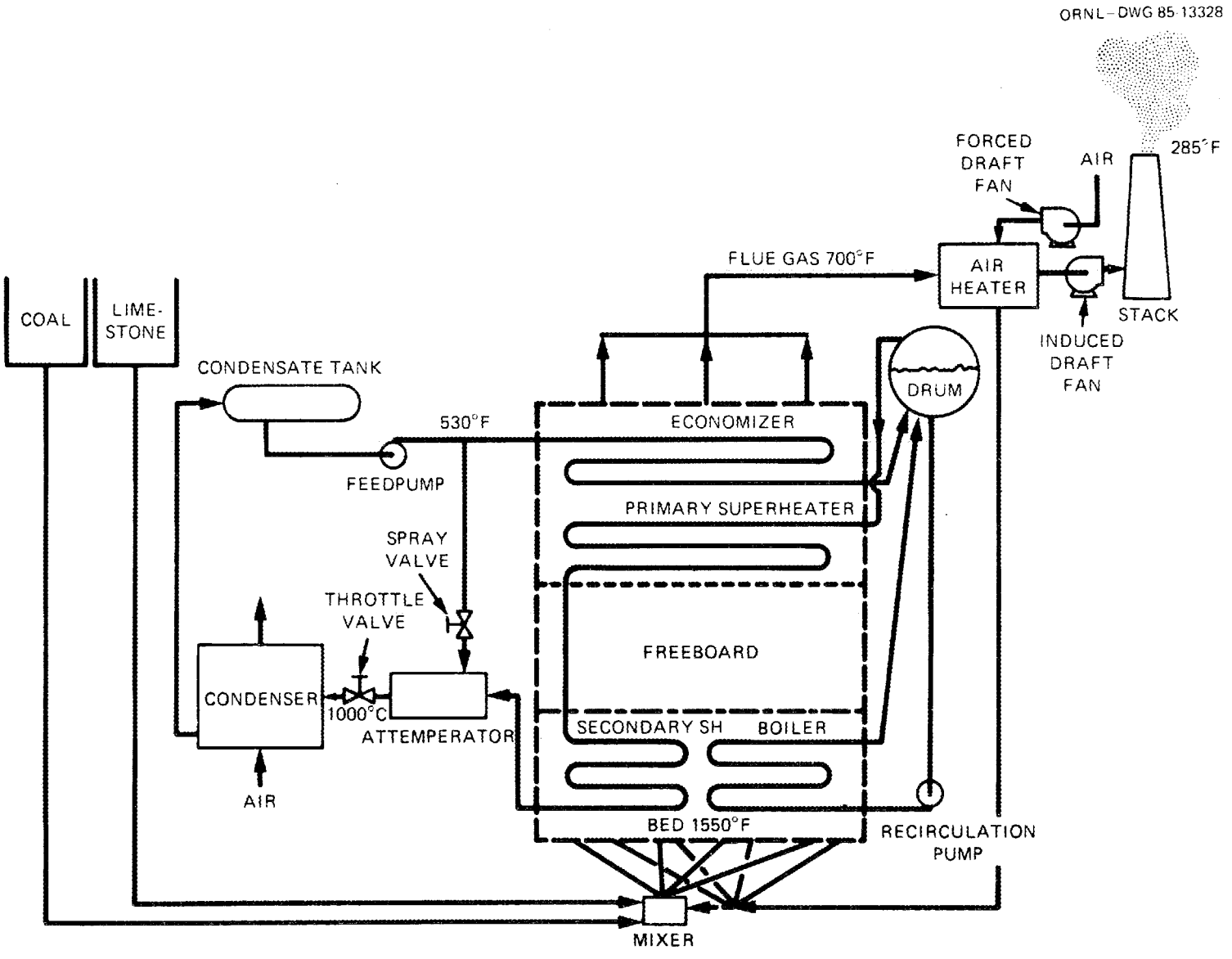

Fig. 1. Model of a fluid-bed pilot plant.

The fourth and final section outputs approximately 150 variables and computed quantities of interest. Eighty of these may be optionally selected for automatic computer plotting--at a considerable reduction in the cost of graphic arts preparation. Some of these graphs are used later in this report.

2. MATHEMATICAL DEVELOPMENT

2.1 WATER/STEAM CIRCUIT

The mathematical foundation of the model may be divided into four broad areas: water and steam circuit, air and gas path, parameter evaluation, and control system. The first three of these will be discussed, and then some open-loop analysis will be reported before taking up the control system and further analysis. Symbols are defined and nominal values of parameters and variables are given in Table 1.

2.1.1 Boiler

The bed evaporator and water wall tubes are combined into a total effective heat transfer surface, A_e. The rate of heat transfer from bed to boiler tubes is

$$Q_e^{in} = a_e A_e K_b (T_b - T_e) \quad , \tag{1}$$

where the heat transfer coefficient, K_b, may be a function of superficial velocity, among other things. Using the nucleate boiling correlation of Thom et al.[2], the rate of heat transfer from tube metal to steam is

$$Q_e^{out} = a_e g_e A_e \exp(p_d/630)(T_e - T_d)^2/[3600(0.072)^2] \quad . \tag{2}$$

Boiler tube metal average temperature is determined by the difference of heat input and output,

$$\frac{d}{dt}(c_m M_e T_e) = Q_e^{in} - Q_e^{out} \quad . \tag{3}$$

Table 1. Symbols and values

Parameter or variable	Description	Value	Source[a]
A_a	Characterized (linearized and normalized) feedwater valve opening	0.95	E
A_b	Bed area	138 ft^2	E
A_d	Characterized furnace inlet damper area	0.95	E
A_e	Boiler heat transfer surface, outside of tubes	734 ft^2	E
A_f	Characterized feedwater valve opening	0.95	E
A_{id}	Characterized ID fan damper opening	0.95	E
A_p	Preheater heat transfer surface	7,900 ft^2	E
A_r	Condenser heat transfer area	24,000 ft^2	E
A_{sp}	Characterized spray-water valve opening	0.5	E
A_{s1}	Primary SH heat transfer surface, outside	2,886 ft^2	E
A_{s2}	Secondary SH heat transfer surface outside	619 ft^2	E
a_b	Fraction of bed fluidized	1	C
a_e	Fraction of boiler heat transfer surface active	1	C
a_{ec}	A constant to give desired heat transfer in economizer	0.3	E
a_{s1}	Fraction of primary SH heat transfer surface active	1	C
a_{s2}	Fraction of secondary SH heat transfer surface active	1	C

Table 1 (continued)

Parameter or variable	Description	Value	Source[a]
a,b,p,q	Parameters in elutriation submodel	N	N
β	Fraction of coal not burned (elutriation, bed discharge)	.01	E
c_c	Coal specific heat	0.25 Btu/lb-°F	C
c_ℓ	Limestone specific heat	0.25 Btu/lb-°F	C
c_m	Metal specific heat	0.14 Btu/lb-°F	C
c_{pa}	Forced draft air specific heat	0.25 Btu/lb-°F	C
c_{pg}	Flue gas specific heat (constant press)	0.25 Btu/lb-°F	C
c_{vg}	Flue gas specific heat (constant volume)	0.18 Btu/lb-°F	C
c_1, c_2	Parameters in elutriation submodel	3.5, 9.9	E
δ_c	Crown height	1 ft	D
E_a	Fractional excess air in furnace	0.18	D
E_{O_2}	Fractional O_2 in flue gas	0.033	C
E_x	Fractional SO_2 removal in region x	0.85 total	D
e_{mf}	Average void fraction in bed at minimum fluidizing velocity	0.7	D
e_1	Nominal average void fraction in bed	0.8	D
F_a	Main steam flow at throttle	65,100 lb/h	C
F_c	Coal feed	6,300 lb/h	C
F_f	Feedwater flow	63,000 lb/h	C

Table 1 (continued)

Parameter or variable	Description	Value	Source[a]
F_g	Flue gas flow	67,000 lb/h	C
F_{id}	Induced draft	67,000 lb/h	C
F_ℓ	Limestone feed	1,600 lb/h	C
F_s	Steam flow from drum to primary SH	63,000 lb/h	C
F_{sp}	Spray water flow	2,100 lb/h	C
$F_{s\ell}$	Spent limestone discharge	1,600 lb/h	C
F_{fa}	Forced draft air	61,000 lb/h	C
f	Fraction of limestone elutriated	0.35	D
f_e	Fraction of bed with boiler surface	0.5	E
f_{s1}	Fraction of bed with superheater surface	0.5	E
f_T	Temperature dependence of SO_2 removal	1.0 at 1,550°F	D
g_e	Geometry factor to convert boiler tube outside area to inside area; ratio inside diameter/outside diameter	0.88	Steam
g_r	Geometry factor for condenser tubes	0.88	Steam
g_{s1}	Geometry factor for primary SH tubes	0.88	Steam
g_{s2}	Geometry factory for secondary SH tubes	0.88	Steam
$\gamma(r)$	Normalized particle size distribution	N	N
H_b	Bed height	4 ft	D

Table 1 (continued)

Parameter or variable	Description	Value	Source[a]
H_c	Coal higher heat value (wet basis as fired)	10,900 Btu/lb	D
H_f	Freeboard height	32 ft	D
H_2	Hydrogen content of coal	0.041 lb/lb	D
h_a	Main steam enthalpy	1,461 Btu/lb	C
h_{ec}	Enthalpy of feedwater entering drum from economizer	592 Btu/lb	C
h_f	Condensate (feedwater) enthalpy	541 Btu/lb	C
h_s	Enthalpy of steam in drum	1,080 Btu/lb	C
h_{s1}	Average enthalpy of steam in primary SH	1,166 Btu/lb	C
h_{s1o}	Enthalpy of steam at primary SH outlet	1,252 Btu/lb	C
h_{s2}	Average enthalpy of steam in secondary SH	1,372 Btu/lb	C
h_{s2o}	Enthalpy of steam at secondary SH outlet	1,493 Btu/lb	C
K(r)	Differential elutriation of limestone	N	N
K	Total fractional elutriation of limestone	0.35	C
K_a	Throttle steam flow constant	0.219	C
K_b	Bed heat transfer coefficient	48 Btu/h-ft^2-°F	D
K_d	Inlet damper air flow constant	0.0907	C
K_f	Feedwater pump constant	0.15	C
K_g	Primary SH gas-side heat transfer coefficient, excluding velocity dependence	0.00024 Btu/h-ft^2-°F-$v_g^{0.6}$	Steam

Table 1 (continued)

Parameter or variable	Description	Value	Source[a]
K_{id}	Induced draft flow constant	0.21	C
K_{pg}	Preheater gas-side heat transfer coefficient, excluding velocity dependence	0.0004 Btu/h-ft^2-°F-$F_{id}^{0.8}$	D
K_{pm}	Preheater air-side heat transfer coefficient, excluding velocity dependence	0.00024 Btu/h-ft^2-°F-$F_{fa}^{0.8}$	D
K_{ra}	Primary SH radiative heat transfer coefficient	N	N
K_{rs}	Condenser steam-side heat transfer coefficient, excluding velocity dependence	0.0054 Btu/h-ft^2-°F-$F_a^{0.8}$	C
K_s	Steam flow constant	0.47	C
K_{sp}	Spray water flow constant	0.00761	C
K_{s1}	Primary SH steam-side heat transfer coefficient, excluding velocity dependence	0.0048 Btu/h-ft^2-°F-$F_S^{0.8}$	Steam
K_{s2}	Secondary SH steam-side heat transfer coefficient, excluding velocity dependence	0.0048 Btu/h-ft^2-°F-$F_S^{0.8}$	Steam
k_{SO_2}	Constant in SO_2 capture formula	0.96	C
L	Load	17.6 MW	C
M_e	Metal mass of boiler and water wall tubes, and drum	28,000 lb	C
M_g	Furnace gas mass	15 lb	C
M_{gc}	Gas mass in primary SH pass	N	N
M_r	Condenser metal mass	26,000 lb	E
$M_{s\ell}$	Bed limestone mass	19,000 lb	E
M_{s1}	Primary SH metal mass	24,000 lb	E

Table 1 (continued)

Parameter or variable	Description	Value	Source[a]
M_{s2}	Secondary SH metal mass	5,150 lb	E
m	Limestone reactivity	0.7	D
μ	Viscosity of flue gas	N	N
p_a	Main steam (throttle) pressure	2,400 psig	D
p_d	Drum pressure	2,585 psig	D
p_f	Feedwater pump pressure	2,885 psig	D
p_{fd}	FD fan pressure	45 Inwg	D
p_i	Air pressure at furnace inlet (before inlet dampers)	45 Inwg	D
p_{id}	ID fan pressure	-13 Inwg	D
p_o	Gas pressure at furnace outlet (preheater inlet)	-2.4 Inwg	D
p_{s1o}	Primary SH outlet pressure	2,508 psig	C
p_{s2o}	Secondary SH outlet pressure	2,400 psig	C
p_S	Partial pressure of SO_2 in flue gas	N	N
$\Delta p_m/F_m^2$	Ratio of rated pressure drop of FD fan and rated flow	0.0063	C
Q_c	Thermal energy generation rate	20 MW	D
Q_e^{in}	Total heat transfer into boiler metal	9 MW	C
Q_e^{out}	Total heat transfer out of boiler metal (to water/steam)	9 MW	C
Q_{ec}	Heat generated in economizer	0.95 MW	C
Q_p^{in}	Total heat transfer from flue gas to preheater metal	2.1 MW	C
Q_p^{out}	Total heat transfer from preheater metal to forced draft air	2.1 MW	C

Table 1 (continued)

Parameter or variable	Description	Value	Source[a]
Q_r^{in}	Total heat transfer from steam to condenser metal	17.7 MW	C
Q_r^{out}	Total heat transfer from condenser metal to cooling air	17.7 MW	C
Q_{s1}^{in}	Total heat transfer into primary SH metal	3.2 MW	C
Q_{s1}^{out}	Total heat transfer out of primary SH metal	3.2 MW	C
Q_{s1c}^{in}	Total convective heat transfer into primary SH metal	3.2 MW	C
Q_{s1r}^{in}	Total radiative heat transfer to primary SH	N	N
Q_{s2}^{in}	Total heat transfer from bed to secondary SH metal	4.5 MW	C
Q_{s2}^{out}	Total heat transfer from secondary SH metal to steam	4.5 MW	C
Q_w	Heat loss in generation of flue gas water vapor	1.1 MW	C
R_{CaS}	Calcium to sulphur mole (atom) ratio in bed	1.6	D
r	Particle radius	N	N
ρ_a	Main stream density	3.14 lb/ft^3	C
$\bar{\rho}_{ag}$	Average air/gas density through furnace	0.034 lb/ft^3	C
ρ_f	Feedwater density	50 lb/ft^3	C
ρ_g	Average flue gas density	0.034 lb/ft^3	C
ρ_o	Gas density at preheater inlet	0.034 lb/ft^3	C

Table 1 (continued)

Parameter or variable	Description	Value	Source[a]
$\bar{\rho}_o$	Average gas density between primary SH and preheater	0.034 lb/ft^3	C
ρ_s	Saturated steam density	8.25 lb/ft^3	C
ρ_ℓ	Bed limestone density	170 lb/ft^3	C
$\rho_{s\ell}$	Spent limestone density	170 lb/ft^3	C
ρ_w	Saturated water density	34 lb/ft^3	C
S_c	Coal input to feed system	6,300 lb/h	C
T_a	Main steam (throttle) temperature	1,000°F	D
T_b	Bed temperature	1,550°F	D
T_c	Mean temperature of limestone/coal/air mixture entering furnace	480°F	D
T_d	Drum steam/water temperature	674°F	D
T_e	Boiler tube mean temperature	676°F	C
T_{ec}	Temperature of water leaving economizer	585°F	C
T_{ex}	Flue gas exhaust (stack) temperature	285°F	D
T_f	Condensate (feedwater) temperature	542°F	D
T_g	Gas temperature at primary SH outlet	717°F	C
$\bar{T}_g$	Average gas temperature in primary SH	1,134°F	C
T_i	Preheater air inlet temperature	55°F	E
T_o	Gas temperature at preheater inlet	717°F	C

Table 1 (continued)

Parameter or variable	Description	Value	Source[a]
T_{pa}	Average air temperature in preheater air pass	266°F	C
T_{pg}	Average gas temperature in preheater gas pass	501°F	C
T_{pm}	Preheater metal mean temperature	391°F	C
T_{ra}	Average air temperature in condenser	248°F	C
T_{ri}	Condenser air intake temperature	55°F	E
T_{rm}	Condenser metal mean temperature	756°F	C
T_{ro}	Condenser air outlet temperature	440°F	D
T_{rs}	Average steam temperature in condenser	771°F	C
T_{s1}	Primary SH mean steam temperature	694°F	C
T_{s2}	Secondary SH mean steam temperature	874°F	C
T_{sm1}	Primary SH mean metal temperature	718°F	C
T_{sm2}	Secondary SH mean metal temperature	1,037°F	C
t_{bu}	Residence time of bubbles in bed	0.6 s	C
t_e	Gas residence time in emulsion phase	1 s	C
t_f	Gas residence time in freeboard	8.3 s	C
τ	Burnup time constant of crushed coal particles	15 s	E
τ_c	Effective fuel transit time through feed system	15 s	E
u_s	Specific energy of steam	765 Btu/lb	C

Table 1 (continued)

Parameter or variable	Description	Value	Source[a]
u_w	Specific energy of water	666 Btu/lb	C
V_b	Bed volume (limestone plus gas)	551 ft^3	C
V_{bu}	Bubble volume fraction	0.33	C
V_d	Drum volume	127 ft^3	D
V_w	Volume of water in drum	67.5 ft^3	C
v_{bu}	Bubble velocity	8.4 ft/s	C
v_g	Gas velocity through primary SH	50 ft/s	Steam
v_{mf}	Minimum fluidizing velocity	1.8 ft/s	D
v_r	Terminal velocity of particle of radius r	N	N
W_v	Total moisture vaporized	3672 lb/h	C
w_a	Moisture fraction of supply air	0.013	Steam
w_c	Moisture fraction of coal	0.09	D

[a]C= calculated from conservation or state relations,
D = AFBC designs or design proposals,
E = estimated,
N = not needed in code,
Steam = Steam/Its Generation and Use.
For further discussion of definition of symbols in this column, see "Model Parameters," page xx.

2.1.2 Primary Superheater

The primary superheater is located above the freeboard where heat transfer is mainly convective, as given by[3],

$$Q_{S1C}^{in} = a_{S1}A_{S1}\ K_g F^{0.6}\dot{g}^{0.6}(\bar{T}_g - T_{Sm1}) \quad , \tag{4}$$

with a small radiative part,

$$Q_{S1r}^{in} = K_{S1r}(T_b^4 - T_{Sm1}^4) \quad , \tag{5}$$

and total,

$$Q_{S1}^{in} = Q_{S1r}^{in} + Q_{S1C}^{in} \quad . \tag{6}$$

Using the Dittus-Boelter relation[4] for turbulent flow in tube bundles, the rate of heat transfer from tube metal to steam is

$$Q_{S1}^{out} = a_{S1}g_{S1}A_{S1}K_{S1}F^{0.8}\dot{s}^{0.8}(T_{Sm1} - T_{S1}) \quad . \tag{7}$$

Conservation of energy in the steam requires

$$Q_{S1}^{out} = F_S(h_{S1O} - h_S) \quad . \tag{8}$$

Average steam conditions in the superheater are related to inlet and outlet conditions by

$$h_{S1} = (h_S + h_{S1O})/2 \quad , \tag{9}$$

$$p_{S1} = (p_d + p_{S1O})/2 \quad , \tag{10}$$

$$T_{S1} = T_{S1}(h_{S1}, p_{S1}) \quad , \tag{11}$$

where the latter functional dependence is obtained from steam tables (Eq. A.1, Appendix). Taking pressure drops in the primary and secondary

superheaters in proportion to power output, the outlet pressure of the primary superheater is obtained from the relationship

$$(p_d - p_{s1o})/(p_d - p_a) = Q_{s1}^{out}/(Q_{s1}^{out} + Q_{s2}^{out}) \quad . \tag{12}$$

Tube metal temperature is determined by the difference of the input and output heat rates,

$$\frac{d}{dt}(c_m M_{s1} T_{sm1}) = Q_{s1}^{in} - Q_{s1}^{out} \quad . \tag{13}$$

2.1.3 Secondary (inbed) Superheater

The development of equations for the secondary superheater parallels that of the primary superheater. The rate of heat transfer from bed to tube metal is

$$Q_{s2}^{in} = a_{s2} A_{s2} K_b (T_b - T_{sm2}) \quad , \tag{14}$$

and from metal to steam,

$$Q_{s2}^{out} = a_{s2} g_{s2} A_{s2} K_{s2} F_s^{0.8} (T_{sm2} - T_{s2}) \quad , \tag{15}$$

with the conservation of energy requirement

$$Q_{s2}^{out} = F_s (h_{s2o} - h_{s1o}) \quad , \tag{16}$$

and average steam conditions related to inlet/outlet conditions by

$$h_{s2} = (h_{s1o} + h_a)/2 \quad , \tag{17}$$

$$p_{s2} = (p_{s1o} + p_a)/2 \quad , \tag{18}$$

$$p_{s2o} = p_a \quad , \tag{19}$$

$$T_{s2} = T_{s2}(h_{s2}, p_{s2}) \quad . \tag{20}$$

The last equation is steam table correlation A.2 of the Appendix. Average tube metal temperature is determined by

$$\frac{d}{dt}(c_m M_{s2} T_{sm2}) = Q_{s2}^{in} - Q_{s2}^{out} \quad . \tag{21}$$

2.1.4 Steam Drum

The saturated steam density in the drum and boiler circuit is determined by the conservation of mass equation,

$$\frac{d}{dt}\left[(V_d - V_w)\rho_s + V_w\rho_w\right] = F_f - F_s \quad . \tag{22}$$

Using steam stables to express water density as a function of steam density, this may be simplified to a function of steam density and water volume only,

$$(\rho_w - \rho_s)\frac{dV_w}{dt} + \left[(V_d - V_w) + V_w\frac{d\rho_w}{d\rho_s}\right]\frac{d\rho_s}{dt} = F_f - F_s \quad . \tag{23}$$

The drum specific internal energy, u_s, is determined by the conservation of energy relationship,

$$\frac{d}{dt}\left[(V_d - V_w)u_s\rho_s + V_w u_w\rho_w\right] = F_f h_{ec} - F_s h_s + Q_s^{out} \quad . \tag{24}$$

Using correlations (Appendix) to express the other thermodynamic variables as functions of steam density, this may be rewritten as a function of ρ_s and V_w only,

$$(u_w\rho_w - u_s\rho_s)\frac{dV_w}{dt} + \left[(V_d - V_w)(\rho_s\frac{du_s}{d\rho_s} + u_s) + V_w(\rho_w\frac{du_s}{d\rho_s} + u_w\frac{d\rho_w}{d\rho_s})\right]\frac{d\rho_s}{dt}$$

$$= F_f h_{ec} - F_s h_s + Q_e^{out} \quad . \tag{25}$$

Feedwater flow to the drum is determined by the pressure differential between the drum and feedwater pump,

$$F_f = K_f A_f \sqrt{(p_f - p_d)\rho_f} \quad . \tag{26}$$

2.1.5 Attemperator

A similar application of conservation of mass and energy gives equations for the attemperator steam density and enthalpy,

$$V_a \frac{d\rho_a}{dt} = F_s + F_{sp} - F_a \tag{27}$$

$$V_a\left(\rho_a - \frac{\partial p_a}{\partial h_a}\bigg|_{\rho_a}\right)\frac{dh_a}{dt}$$

$$= F_s h_{s2o} + F_{sp} h_f - F_a h_a - (F_s + F_{sp} - F_a)\left[h_a - \frac{\partial p_a}{\partial \rho_a}\bigg|_{h_a}\right] \quad . \tag{28}$$

Because of the relatively small volume of the attemperator V_a, the numerical solution of these equations tends to require smaller time steps than the other differential equations (the system is mathematically stiff), which increases computer time and cost. Also because of the small volume, physical steam conditions in the attemperator tend to remain in instantaneous equilibrium (i.e., the left-hand sides of the equations containing V_a are comparatively small). By neglecting them, the attemperator equations reduce to simpler algebraic relations that decrease computer solution time.

Spray water flow is a function of the pressure differential between the attemperator and feedwater pump,

$$F_{sp} = K_{sp} A_{sp} \sqrt{(p_f - p_a)\rho_f} \quad , \tag{29}$$

and steam flow through the superheaters is related to the differential across them,

$$F_s = K_s\sqrt{(p_d - p_a)\rho_s} \quad . \tag{30}$$

Critical flow is assumed through the throttle valve to the condenser, and the mainsteam flow is then

$$F_a = K_a A_a \sqrt{p_a \rho_a} \quad . \tag{31}$$

In the model, the attemperator was placed after the secondary superheater in anticipation of a possible tertiary unit. Depending on plant design, the attemperator may be relocated ahead of the secondary superheater.

2.1.6 Air-Cooled Condenser

The turbine-generator set is simulated here with an effective heat transfer coefficient to include any desuperheating and condensate subcooling. Rate of heat transfer from steam to condenser tube metal is given by

$$Q_r^{in} = g_r A_r K_{rs} F^{0.8} (T_{rs} - T_{rm}) \tag{32}$$

and from metal to air by

$$Q_r^{out} = A_r K_{ra} F^{0.6} (T_{rm} - T_{ra}) \quad , \tag{33}$$

where steam and air temperatures T_{rs} and T_{ra} are averages of the inlet and outlet values,

$$T_{rs} = (T_a + T_f)/2 \tag{34}$$

$$T_{ra} = (T_{ri} + T_{ro})/2 \quad . \tag{35}$$

Conservation of energy on the steam side relates heat removal to change in enthalpy,

$$Q_r^{in} = F_a(h_a - h_f) \quad . \tag{36}$$

Condensate temperature and enthalpy T_f and h_f are correlated from steam tables. On the air side, with the small volume of air at nearly incompressible flow, conservation of energy relates heat transfer to the flow of internal energy in the equation,

$$Q_r^{out} = F_r c_{pa}(T_{ro} - T_{ri}) \quad . \tag{37}$$

The system load is the heat removed by air cooling,

$$L = Q_r^{out} \quad . \tag{38}$$

The condenser metal temperature is determined by net heat input,

$$\frac{d}{dt}(c_m M_r T_{rm}) = Q_r^{in} - Q_r^{out} \quad . \tag{39}$$

2.1.7 Economizer

Assuming only a small percentage of power is generated in the economizer, it is approximated as a fixed fraction of the primary superheater power,

$$Q_{ec} = F_f\ (h_{ec} - h_f) \cong a_{ec} Q_{sl}^{out} \quad , \tag{40}$$

where a_{ec} is a constant.

2.2 AIR AND GAS PATH

2.2.1 Air Preheater

Heat transfer from flue gas to metal in a regenerative air preheater is given by[5]

$$Q_p^{in} = A_p K_{pg} F_{id}^{0.8}(T_{pg} - T_{pm}) \quad . \tag{41}$$

For the small volume of gas at nearly incompressible flow, conservation of energy relates heat transfer to the flow of internal energy in the equation,

$$Q_p^{in} = c_{pg}F_{id}(T_o - T_{ex}) \quad . \tag{42}$$

Rate of heat transfer from metal to air is

$$Q_p^{out} = A_p K_{pm} F_{fa}^{0.8}(T_{pm} - T_{pa}) \quad . \tag{43}$$

Applying conservation of energy to mass flow on the air side,

$$Q_p^{out} = (c_{pa}F_{fa} + F_c c_c + F_\ell c_\ell)(T_c - T_i) \quad , \tag{44}$$

in which is included the heat required to raise coal and limestone feed from ambient air temperature, T_i, to furnace inlet air temperature, T_c. Preheater metal temperature is found from conservation of energy,

$$\frac{d}{dt}(c_m M_p T_{pm}) = Q_p^{in} - Q_p^{out} \quad . \tag{45}$$

Gas and air temperatures are averages of inlet and outlet conditions,

$$T_{pg} = (T_o + T_{ex})/2 \tag{46}$$

$$T_{pa} = (T_i + T_c)/2 \quad . \tag{47}$$

2.2.2 Forced Draft Flow

Supply air is related to the pressure differential between the FD fan and the furnace plenum upstream of the inlet dampers by the equation,

$$F_{fa} = F_m\sqrt{(p_i - p_{fd})/\Delta p_m} \quad , \tag{48}$$

where Δp_m is rated pressure drop at rated air flow F_m.

2.2.3 Bed

The firing rate in the bed is treated as a first order lag to account for delay between injection and consumption of crushed coal particles,

$$\frac{dQ_c}{dt} = [(1 - \beta)F_c H_c - Q_c]/\tau \quad . \tag{49}$$

The parameter β is the net fraction of coal lost through elutriation and bed discharge, and $(1 - \beta)F_c$ is net coal burned (includes recycle, if any). τ is the time constant for burnup of crushed coal particles.

The bed temperature is determined by conservation of energy,

$$\frac{d}{dt}\left[(M_{s\ell}c_\ell + M_g c_{vg} + M_c c_c)T_b\right]$$

$$= (F_\ell c_\ell + F_c c_c)T_c - F_{s\ell} c_\ell T_b + F_{fa} c_{pa} T_c$$

$$- \beta F_c c_c T_b - F_g c_{pg} T_b + Q_c - Q_w - Q_{s2}^{in} - Q_e^{in} - Q_r \quad . \tag{50}$$

The left-hand side is the rate of change of bed heat content and is the sum of limestone, furnace gas, and coal internal energies. The latter two are small components; the mass of the limestone may change slowly, if at all, and the left-hand side may be simplified to a derivative of bed temperature only.

The heat input and removal terms on the right are, in order, the heat content of incoming limestone and coal, heat of discharged (spent) limestone, heat of incoming air, heat of discharged coal, heat from burning coal, heat to vaporize coal moisture, heat transferred to secondary superheater, heat transferred to boiler, and radiative heat transfer.

Three sources of vaporized moisture are included. The first is water formed as a combustion product; with H_2 as the hydrogen concentration in coal, this is $8.94H_2$[6]. The other two sources are the moisture fraction in coal w_c and in supply air w_a. Total moisture vaporized is then

$$W_V = 8.94H_2Q_c/H_c + w_cQ_c/H_c + w_aF_{fa} \quad , \tag{51}$$

and the heat loss at 1040 Btu/lb is

$$Q_W = 1040W_V \quad . \tag{52}$$

Coal feed is simulated as a first-order lag to account for transport delays,

$$\frac{dF_c}{dt} = (S_c - F_c)/\tau_c \quad , \tag{53}$$

where τ_c is the transport time delay.

The limestone feed required for a calcium to sulphur ratio R_{CaS} is related to coal feed F_c, coal sulphur concentration C_S, and calcium carbonate concentration of limestone C_{CaCO_3} by the expression

$$F_\ell = 3.12(C_S/C_{CaCO_3})R_{CaS}F_c \quad , \tag{54}$$

where the numerical constant evolves from ratios of the molecular weights of Ca, $CaCO_3$, and S.

To maintain bed level, net output of spent limestone equals input,

$$F_{s\ell} = F_\ell \quad . \tag{55}$$

Simulation of SO_2 capture in the bed and freeboard parallels in part the modeling work of others.[7,8] Sorption in the bed is split into emulsion, bubble, and crown parts. The elutriated limestone is associated with the bubbles, and bubble-phase capture may occur in that

fraction f of the limestone. Emulsion-phase capture occurs in the remaining 1-f of the limestone. Freeboard capture may additionally occur in the elutriated fraction. The crown, where recirculation and some disentrainment of solids occurs, is treated as part of the bed and is subtracted from the height of the freeboard.

The basic equation is

$$\frac{dp_S}{dt} = -k_{SO_2}(mR_{CaS} - E)p_S f_T \quad , \tag{56}$$

in which the combination of gaseous sulphur (partial pressure p_S) with solid limestone is approximated as a simple, first-order reaction. Integration over the appropriate gas residence time in each region results in the following expressions that relate fractional capture E to calcium-to-sulphur ratio, gas residence time, t, and bed temperature, T_b.

a. Bed emulsion phase:

$$E_e = \frac{mR_{CaS}[1 - \exp(-k_{SO_2} f_T(1 - f)(mR_{CaS} - 1)t_e)]}{mR_{CaS} - \exp[-k_{SO_2} f_T(1 - f)(mR_{CaS} - 1)t_e]} \quad , \tag{57}$$

$$t_e = (H_b + \delta_c)/(v_s/e_1) \quad . \tag{58}$$

b. Bed bubble phase:

$$E_b = \frac{mR_{CaS}[1 - \exp(-k_{SO_2} f_T f(mR_{CaS} - 1)t_{bu})]}{mR_{CaS} - \exp[-k_{SO_2} f_T f(mR_{CaS} - 1)t_{bu}]} \quad , \tag{59}$$

$$t_{bu} = (H_b + \delta_c)/v_{bu} \quad , \tag{60}$$

$$v_{bu} = (v_s - v_{mf})/V_{bu} + v_{mf} \quad , \tag{61}$$

$$V_{bu} = 1 - (1 - e_1)/(1 - e_{mf}) \quad . \tag{62}$$

c. Total bed:

$$E_{eb} = E_e + E_b \quad . \tag{63}$$

d. Total capture including freeboard:

$$E_t = \frac{\dfrac{mR_{CaS}(1 - E_{eb})}{mR_{CaS} - E_{eb}} - \exp[-k_{SO_2} f_T f(mR_{CaS} - 1)t_f]}{\dfrac{1 - E_{eb}}{mR_{CaS} - E_{eb}} - \exp[-k_{SO_2} f_T f(mR_{CaS} - 1)t_f]} \quad , \tag{64}$$

$$t_f = (H_f - \delta_c)/v_s \quad . \tag{65}$$

The overall temperature dependence of the multireaction capture process is approximated by an empirical correlation based on limited data[7,8],

$$f_T = \exp[-(T_b - 1550)/115]^2 \quad . \tag{66}$$

The parameter k_{SO_2} was evaluated from data[8] as shown in Fig. 2a. Though the SO_2 source distribution may be peaked toward the lower part of the bed, a uniform source was used here because it was felt that greater detail was not justified by available data. The shape of the source distribution tends in any case to be submerged in the experimental constant k_{SO_2}.

Fractional SO_2 removal is a function of elutriation f, and the following submodel was developed to predict elutriation. The correlation of Merrick and Highley[9] is used to describe the rate of elutriation of particles of radius r,

$$K(r) = \rho_g v_s p \exp[-q(v_r/v_s)^{0.5}(v_{mf}/(v_s - v_{mf}))^{0.25}] \quad . \tag{67}$$

Using the Stokes formula for terminal velocity as a function of particle radius, the above expression reduces to a simple exponential function of particle radius,

$$K(r) = \rho_g v_s p \exp[-rq(2(\rho_{s\ell} - \rho_g)/(9\mu v_s))^{0.5}$$

$$(v_{mf}/(v_s - v_{mf}))^{0.25}] \quad . \tag{68}$$

A normalized Rosin-Rammler-type correlation is used for the particle size distribution,

$$\Upsilon(r) = a\exp(-r/b) \quad . \tag{69}$$

Total fractional elutriation as a function of superficial velocity is then the integral of the product of the two correlations,

$$K = \frac{A_b \int_0^\infty \Upsilon(r)K(r)dr}{M_b \int_0^\infty \Upsilon(r)dr}$$

$$= \frac{v_s^{1.5}(v_s - v_{mf})^{0.25}}{[c_1 + c_2 v_s^{0.5}(\bar{v}_s - v_{mf})^{0.25}]} \quad . \tag{70}$$

As a result of the integration, eight parameters in the original correlations coalesce into a single pair of unknowns c_1 and c_2 that may be readily evaluated from two experimental measurements of total elutriation in a specific bed. The function is plotted in Fig. 2b for beds with high and low elutriation. The curves show elutriation to be proportional to the square of superficial velocity near the minimum fluidizing velocity (mfv) and proportional to the first power of velocity away from mfv.

Excess air is calculated from forced draft flow and firing rate by the relationship

$$E_a = (F_{fa} - Q_c \times 7.57 \times 10^{-4})/(Q_c \times 7.57 \times 10^{-4}) \quad , \tag{71}$$

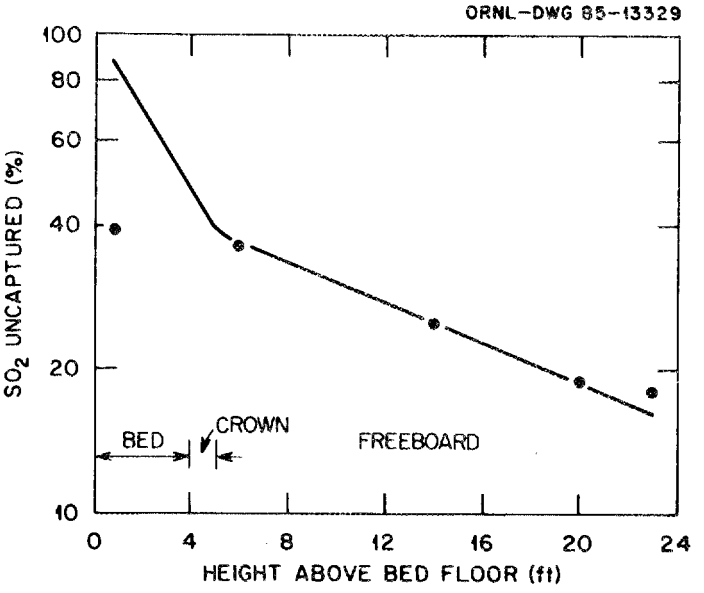

Fig. 2a. SO_2 in flue gas. Dots (●), experimental data[8]; solid curve, model prediction.

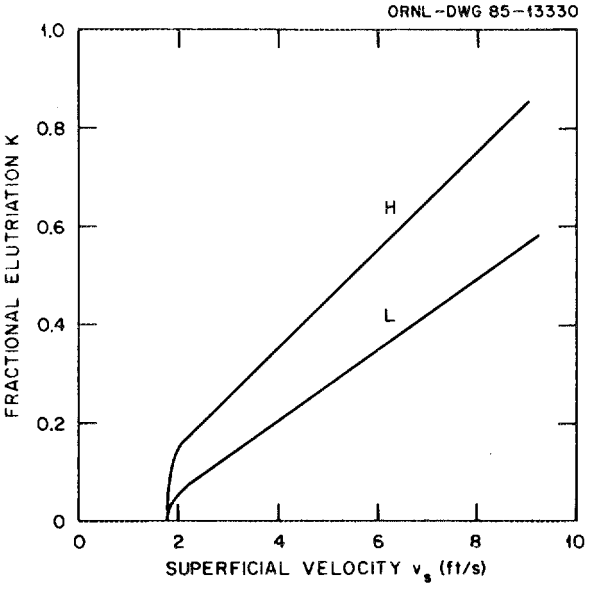

Fig. 2b. Total elutriation as a function of superficial velocity. Curve H is fit to a postulated pair of measurements K = 0.35 at 4 ft/s and K = 0.75 at 8 ft/s. Curve L with lower elutriation is fit to K = 0.2 at 4 ft/s and K = 0.5 at 8 ft/s.

where the numerical constant is the stoichiometric air required for coal with 43% volatile content, dry ash-free basis.

Expressed as O_2 in the flue gas,

$$E_{O_2} = 0.232(F_{fa} - Q_c \times 7.57 \times 10^{-4})/F_g \quad . \tag{72}$$

Load-following by slumping and fluidizing compartments is simulated by inputting the total fractions of the bed f_e and f_{s2} that contain boiler and superheater surface, and then selectively varying the active boiler and superheater surface fractions a_e and a_{s2} and the fraction of bed fluidized $a_b = f_e a_e + f_{s2} a_{s2}$. Individual compartments may be any portion of the bed area. By a minor change of the model, active bed area and transfer surface can be decoupled in order to simulate the alternative load-following procedure of exposing transfer surface by varying bed mass and height without slumping.

2.2.4 Convection Zone

In the convective pass through the primary superheater, the gas volume and mass are small, and the equilibrium conservation of energy relation is used,

$$\frac{d}{dt}(c_{vg} M_{gc} \bar{T}_g)$$

$$= F_g c_{pg}(T_b - T_g) - a_{s1} A_{s1} K_g F^{0.6} \dot{g}^{0.6} (\bar{T}_g - T_{sm1})(1 + a_{ec}) = 0 \quad . \tag{73}$$

The first term on the right is heat removal from the gas between superheater inlet and outlet, and the second is heat transferred to the tube metal. The a_{ec} term is approximate economizer heat transfer described previously. Gas temperature, $\bar{T}_g$, is the average of inlet (bed outlet) temperature, T_b, and outlet temperature, T_g.

Manipulation of primary superheater surface (dampering) is simulated by varying the active surface fraction a_{s1} and the gas flow area.

Flue gas mass flow is the sum of supply air and combusted fuel,

$$F_g = F_{fa} + Q_c/H_c \quad . \tag{74}$$

Fluidizing air flow is predicted from the pressure differential between furnace inlet and outlet and the average gas density,

$$F_{fa} \propto \sqrt{(p_i - p_o)\bar{\rho}_{ag}} \sim \sqrt{(p_i - p_o)(p_i + p_o)/2}$$

$$= A_d K_d \sqrt{p_i^2 - p_o^2} \quad , \tag{75}$$

where the perfect gas law has been used.

Flue gas density and temperature at the preheater are obtained from conservation of mass and energy in the duct volume, V_o, between primary superheater and air preheater

$$\frac{d}{dt}(V_o\bar{\rho}_o) = F_g - F_{id} \quad , \tag{76}$$

$$\frac{d}{dt}(c_{vg}V_o\bar{\rho}_o\bar{T}_o) = c_{pg}(F_gT_g - F_{id}T_o) \quad , \tag{77}$$

where the average density and temperature in this volume are related to inlet and outlet values,

$$\bar{\rho}_o = (\rho_g + \rho_o)/2 \quad , \tag{78}$$

$$\bar{T}_o = (T_g + T_o)/2 \quad . \tag{79}$$

Preheater inlet pressure is calculated from the perfect gas law,

$$p_o = \rho_o \frac{R}{\bar{M}} T_o^{abs} \quad . \tag{80}$$

2.2.5 Induced Draft Flow

Stack gas flow is calculated from the pressure differential between preheater inlet and ID fan inlet,

$$F_{id} = A_{id}K_{id}\sqrt{p_o^2 - p_{id}^2} \quad . \tag{81}$$

2.3. SUMMARY OF STATE VARIABLE EQUATIONS

There are twelve variables represented by differential equations.

Variable	Description	Equation
T_e	Boiler metal temperature	(3)
T_{sm_1}	Primary SH metal temperature	(13)
T_{sm_2}	Secondary SH metal temperature	(21)
ρ_s	Drum steam density	(23)
V_w	Drum water volume	(25)
T_{rm}	Condenser metal temperature	(39)
T_{pm}	Preheater metal temperature	(45)
Q_c	Coal burning rate	(49)
T_b	Bed temperature	(50)
F_c	Coal feed rate	(53)
ρ_o	Flue gas density	(76)
T_o	Flue gas temperature	(77)

There are, in addition, approximately 140 variables derived from algebraic relations and correlations. These include pressures, flows, heat balance information such as heat exhausted through the stack and spent bed material and the quantities of heat stored in system components (evaporator metal, bed material, etc.).

3. PARAMETERS

Parameters for the model are based in part on a review of AFBC designs or design proposals for plants in the 20- to 25-MW range. These are marked D in the table. In other cases, as for various heat transfer coefficients, values were obtained from standard design practice, e.g., Steam/Its Generation and Use.[3] These are marked Steam in the table. The flow dependence of transfer coefficients has been split off because it varies in a transient calculation. For a coefficient of the type $h = kF^n$, where F^n is the flow dependence, the value in Table 1 is k; the value obtained from the design manual is h. Quantities marked N are not needed in the computer code.

Given the data in these sources, most of the other required parameters can be calculated from conservation of mass and energy relations plus standard steam table correlations. These calculated values are marked C in the table.

After these sources of what are believed to be sound parameter values were exhausted, a few parameters remained that had to be estimated from best judgment. These are mostly the magnitudes of heat transfer surface areas and component masses. They are marked E in the table.

4. OPEN-LOOP ANALYSIS

4.1 INHERENT DYNAMICS

Before taking up the control system, calculations will be described in which the model was used to investigate generic open-loop (without controls) behavior of the plant. Twelve parameters were individually reduced by 1%, and the system responses were determined. The varied parameters are among those which may be collectively manipulated to control the boiler. Varying them individually provides insight into their separate functions as well as the ways in which they may tend to support or interfere with each other when coupled in a control system. A number of interesting observations can be made about the natural dynamic behavior of the fluid-bed system as presently modeled.

Table 2 lists initial values of the varied parameters and some of the important variables that were analyzed. Table 3 lists the changes in the variables that result from each of the parameter variations. Entries in Table 3 occur in pairs; the upper number of each pair is in the units indicated at the head of the column, and the lower number is the percentage of change. For example, a 1% reduction in coal feed rate produces an increase in evaporator power generation of 0.019 MW (upper number of pair) or 0.22% (lower number). The percentage of change is referenced to evaporator power, not to total power. For ease of presentation in Table 3, the numbers were rounded to two significant figures. Again for convenience, parameter variations of 1% were made. For example, a variation of 5% would produce changes in the variables approximately five times as large. Since a drum-type boiler is inherently unstable unless the drum water level is regulated, a level controller is operating in these otherwise open-loop simulations. Effects of the controller will be apparent in some of the cases discussed. In these studies the power was set at 15 MW.

In the first case in Table 3, coal feed was reduced by 1%. Figures 3a through 3g show the transient response to the disturbance. Figure 3a shows total power; Figs. 3b through 3d show power generation

Table 2. Nominal values of parameters and variables

Parameter	Initial value
Coal feed	1.28 lb/s
Air inlet damper	90% open
FD fan pressure	45.0 Inwg
Flue gas damper	90% open
ID fan pressure	-14.7 Inwg
Feedpump pressure	2982 psig
Attemperator valve	50% open
Throttle valve	90% open
Evaporator surface	720 ft^2
Primary superheater surface	4000 ft^2
Secondary superheater surface	1000 ft^2
Condenser air flow	145 lb/s
Variable	
Evaporator power	8.66 MW
Primary superheater power	3.04 MW
Secondary superheater power	2.88 MW
Condenser load (total power)	14.7 MW
Stack loss	1.06 MW
Bed temperature	1550°F
Primary superheater metal temperature	926°F
Secondary superheater metal temperature	1200°F
Drum temperature	688°F
Drum pressure	2829 psig
Throttle steam temperature	1000°F
Throttle steam pressure	2605 psig
Throttle steam flow	13.4 lb/s
Fluidizing air flow	13.2 lb/s
Furnace gas temperature	713°F
Stack gas temperature	285°F

Table 3. Sensitivity of AFBC state variables to changes in selected system parameters. Change (upper datum) and percent change (lower datum) in state variable.

Parameter reduced by 1%	Evap. power (MW)	Prim. S.H. power (MW)	Sec. S.H. power (MW)	Condens. load (MW)	Stack loss (MW)	Bed temp. (°F)	Prim. S.H. metal temp. (°F)	Sec. S.H. metal temp. (°F)	Drum temp. (°F)	Drum press. (psig)	Throttle steam temp. (°F)	Throttle steam press. (psig)	Throttle steam flow (lb/s)	Fluid. air flow (lb/s)	Furnace gas temp. (°F)	Stack gas temp. (°F)
Coal feed	0.019	-0.029	-0.15	-0.16	0.0058	-2.2	3.4	10	-4.4	-78	12	-74	-0.51	0.002	5.3	1.8
	0.22	-0.97	-5.3	-1.1	0.55	-0.14	0.37	0.76	-0.64	-2.8	1.2	-2.9	-3.8	0.015	0.74	0.62
Air inlet damper	-0.0018	-0.0091	0.023	0.011	-0.011	0.25	-1.7	-1.6	0.47	8.5	-2.2	7.9	0.064	-0.1	-3.1	-1.5
	-0.021	-0.3	0.8	0.075	-1.1	0.016	-0.18	-0.12	0.068	0.3	-0.22	0.3	0.48	-0.77	-0.43	-0.51
FD fan pressure	-0.014	-0.051	0.13	0.062	-0.062	1.1	-9.3	-9.4	2.7	48	-12.8	45	0.37	-0.55	-17	-8.0
	-0.17	-1.7	4.5	0.42	-5.9	0.071	-1.0	-0.71	0.39	1.7	-1.3	1.7	2.7	-4.1	-2.4	-2.8
Flue gas damper	-0.0004	-0.0021	0.0054	0.0027	-0.0027	0.1	-0.38	-0.3	0.11	2.0	-0.51	1.8	0.015	-0.024	-0.72	-0.34
	-0.0046	-0.069	0.19	0.018	-0.25	0.006	-0.041	-0.023	0.016	0.071	-0.051	0.069	0.11	-0.18	-0.1	-0.12
ID fan pressure	-0.0046	-0.035	0.088	0.046	-0.046	1.2	-6.3	-5.8	1.8	33	-8.3	30	0.24	-0.4	-12	-5.7
	-0.053	-1.2	3.1	0.31	-4.4	0.077	-0.68	-0.44	0.27	1.2	-0.83	1.2	1.8	-3.0	-1.7	-2.0
Feedpump pressure	0.0058	0.0002	-0.0064	-0.0005	0.0005	0.4	0.35	0.9	-0.21	-3.7	1.8	-3.5	-0.035	0	0.33	0.12
	0.067	0.0066	-0.22	-0.0034	0.047	0.026	0.038	0.068	-0.031	-0.13	0.18	-0.13	-0.26	0	0.046	0.042
Attemperator valve	0.0015	0.0001	-0.0016	-0.0001	0.0001	0.1	0.09	0.2	-0.05	-0.9	0.4	-0.9	-0.008	0	0.08	0.03
	0.017	0.0033	-0.056	-0.00068	0.0094	0.0065	0.0097	0.0015	-0.0073	-0.032	0.04	-0.035	-0.06	0	0.011	0.01
Throttle valve	-0.034	-0.0031	0.038	0.0012	-0.0012	-1.6	-0.98	-4.7	1.9	33	-5.0	36	0.11	0	-0.77	-0.27
	-0.39	-0.1	1.3	0.0081	-0.11	-0.1	-0.11	-0.36	0.27	1.2	-0.5	1.4	0.79	0	-0.11	-0.095
Evaporator surface	-0.001	0.019	-0.023	-0.004	0.004	7.7	3.9	9.5	-0.98	-18	7.5	-16	-0.15	0	2.5	0.89
	-0.012	0.61	-0.79	-0.027	0.4	0.5	0.42	0.72	-0.14	-0.62	0.75	-0.59	-1.1	0	0.36	0.31
Primary S.H. surface	0.0017	-0.013	0.0069	-0.005	0.005	0.2	0.73	-0.4	0.01	0.2	-0.81	0	0.007	0	3.7	1.3
	0.02	-0.42	0.24	-0.034	0.46	0.013	0.79	-0.03	0.0015	0.0071	-0.0081	0	0.052	0	0.52	0.45
Secondary S.H. surface	-0.0004	0.0049	-0.0035	0.001	-0.001	0.4	-0.61	-1.6	0.46	8.2	-3.6	7.3	0.072	0	-0.96	-0.33
	-0.0046	0.16	-0.12	0.0068	-0.1	0.026	-0.066	-0.12	0.067	0.29	-0.36	0.28	0.54	0	-0.13	-0.12
Condenser air flow	-0.06	-0.0016	0.067	0.005	-0.005	-4.1	-3.7	-9.4	2.0	37	-9.0	34	0.27	0	-3.6	-1.3
	-0.69	-0.053	2.33	0.034	-0.5	-0.26	-0.4	-0.71	0.3	1.3	-0.9	1.3	2.0	0	-0.51	-0.45

in the evaporator, primary (above-bed) superheater, and secondary (in-bed) superheater, respectively. The total power level requires 0.5 h to approach a new equilibrium. Because of its high nucleate boiling heat transfer coefficient and comparatively small metal mass and heat capacity, the evaporator approaches equilibrium in about a third of this time. Sixty percent of the power is generated in the evaporator, and with the strong heat transfer coefficient, the bed temperature (Fig. 3e) follows the evaporator temperature fairly closely despite the substantial bed heat capacity. The superheaters with smaller transfer coefficients (especially the primary superheater) and larger time constants than the evaporator have a more sluggish effect on power output. Further analysis of the dynamic influence of bed heat capacity is given later.

Under load changes, boilers have the natural tendency to either store heat in or release heat from the evaporators and superheaters. In conventional boilers, convective superheaters (such as the primary superheater in the present study) typically store heat under load increase and release it under load decrease. This deteriorates the ability of the plant to respond promptly to the load change because increased firing initially goes partially into storage rather than load. Conventional radiant superheaters, on the other hand, tend to release heat under load increase, which assists the control system by providing a relatively prompt supply of temporary additional heat.

The superheater in the bed of an AFBC falls in neither the convective nor the radiant category, and its load-following behavior needs to be determined. The present simulation provides some information. After a 1% reduction in coal feed and corresponding reduction in load (air cooling), Fig. 3a shows the power level undershooting by about 25% before reaching a new equilibrium. The undershoot is the consequence of the system storing an increased amount of heat in metal and fluid masses. At equilibrium, the bed superheater, primary superheater, and evaporator heat storages increased by 0.8%, 0.39%, and 0.3%, respectively; the bed heat storage decreased by -0.14%; and the net change in system heat storage was positive, +0.3%. Thus, in

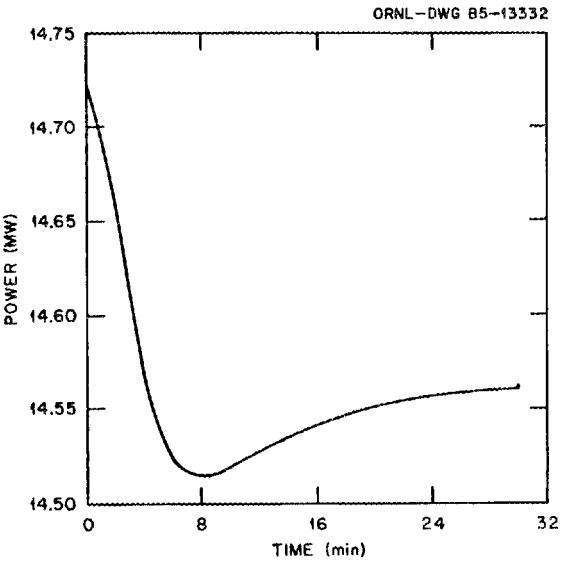

Fig. 3a. Open-loop response to 1% reduction of coal feed. Total power generation.

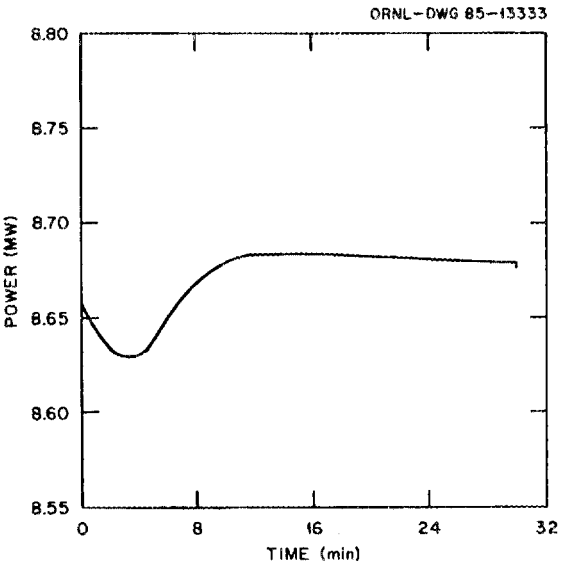

Fig. 3b. Power generation in evaporator.

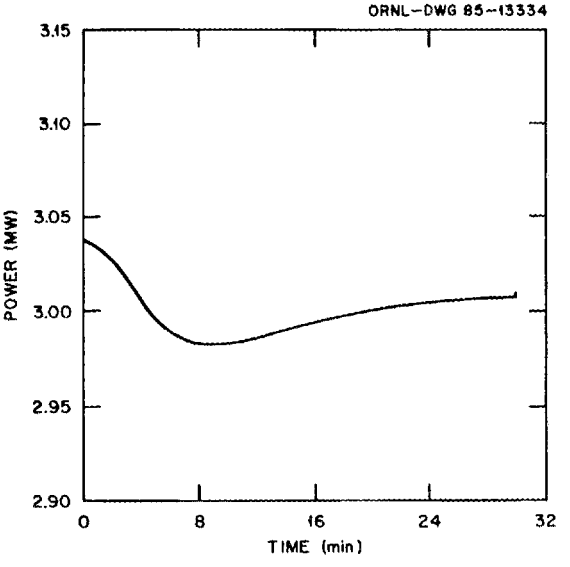

Fig. 3c. Power generation in primary (above-bed) superheater.

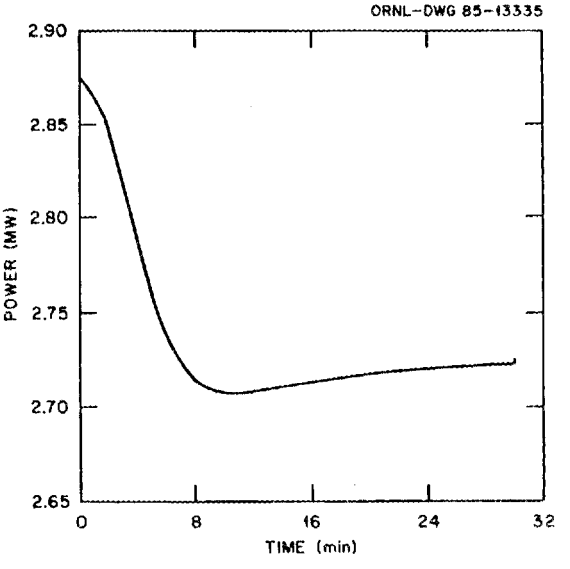

Fig. 3d. Power generation in secondary (in-bed) superheater.

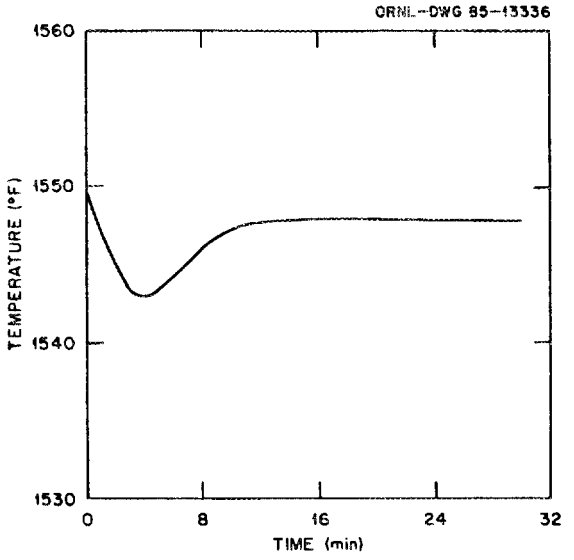

Fig. 3e. Bed temperature.

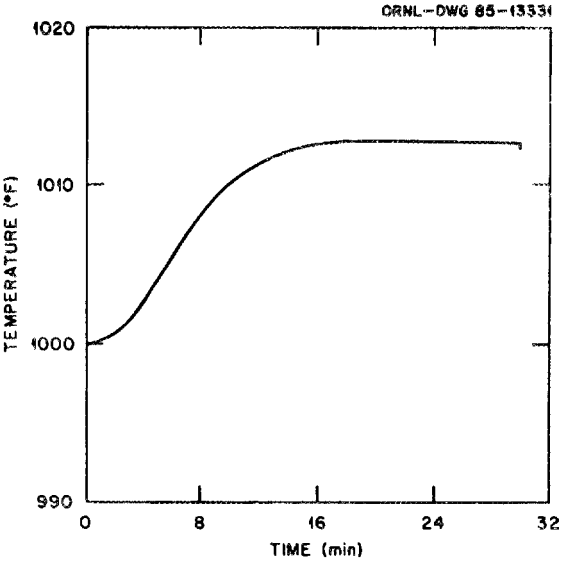

Fig. 3f. Throttle steam temperature.

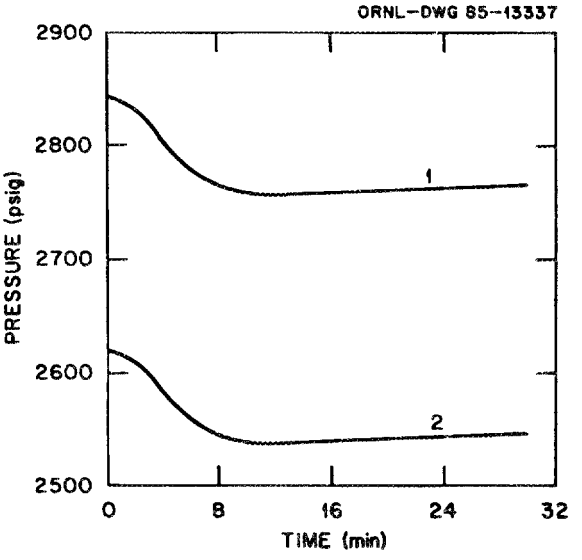

Fig. 3g. Drum pressure (1) and throttle steam pressure (2).

the fluid-bed configuration currently modeled, the bed superheater appears to have beneficial heat storage and load-following dynamics, as does the total system heat storage.

Figures 3b through 3d and related data in Table 3 show that with reduced coal feed and load there is a shift in power distribution among the evaporator and superheaters; generation in the evaporator increases while that in the superheaters decreases. A similar pattern occurs in conventional boilers and can lead to large temperature shifts if not controlled. In the case of the fluid-bed system, the values in Table 3 indicate that much of the redistribution occurs between the evaporator and bed superheater--that is, the redistribution occurs largely within the bed, the net change in bed power generation is relatively small, and the bed temperature change is correspondingly small. In Fig. 3e the bed temperature decreases approximately 7°F during the first 5 min of the transient and recovers to a final equilibrium 2°F below initial value. The 1% reduction in firing rate results in a bed temperature change of only -0.14%.

Decreased coal feed to the boiler causes a reduction of drum pressure and steam flow rate. Because of thermohydraulic nonlinearities, the decrease in flow is about 4% compared with the 1% reduction in heat generation. Consequently, throttle steam temperature (Fig. 3f) increases by 12°F, close to the limit manufacturers allow for turbines, and the inherent mismatch between change in firing rate and desired change in steam flow requires control as in conventional plants.

Table 3 further shows that the smaller size of the secondary superheater makes its metal temperature, T_{sm_2}, more sensitive than the primary superheater metal temperature, T_{sm_1}, to fluctuations in steam flow. With approximately equal heat generation in the two units, the ratio of changes in metal temperatures is roughly proportional to the inverse ratio of heat transfer surface areas,

$$\frac{\Delta T_{sm_2}}{\Delta T_{sm_1}} \propto \frac{A_{s_1}}{A_{s_2}} .$$

On a percentage basis, the quantities showing greatest sensitivity to the 1% change in coal feed are secondary superheater power generation (-5.3%), steam flow rate (-3.8%), throttle pressure (-2.9%), drum pressure (-2.8%), and throttle steam temperature (1.2%). (Throttle and drum pressures are shown in Fig. 3g) One of the least sensitive quantities is bed temperature (-0.14%); this insensitivity persists throughout the disturbances listed in Table 3. Because of its effect on SO_2 removal, bed temperature will be one of the more important variables. The noted tendency of evaporator and bed superheater power generation rates to respond in opposition acts to buffer the bed temperature and inherently stabilize SO_2 removal against system upsets.

At the end of 30 min of simulated plant operation, the transient calculation was terminated and the final equilibrium conditions computed. Equilibrium values were plotted, without lifting the Calcomp plotter pen, at the ends of the curves in Figs. 3a through 3g. The resulting small vertical tail on each curve gives the deviation from final equilibrium remaining when the transient was terminated. Examination of the curves in the various figures shows that the course of the transient is qualitatively clear after about the first ten minutes. Beyond that point is a slow, shallow, and predictable approach to equilibrium. For the remaining cases in Table 3, the transient calculations where therefore terminated at 10 min and the new equilibria determined, reducing computer time to one third. Plots of these cases need not be included here. Selected additional cases from column 1 of Table 3 will be discussed.

4.1.1 Air Inlet Damper Setting

Closing the inlet damper by 1% reduces air intake, stack loss, and the flow-dependent heat transfer coefficient of the primary superheater. There results a shift in heat transfer from the primary to the secondary superheater, and bed temperature increases slightly. Although drum temperature and pressure increase, heat transfer in the evaporator declines (in opposition to the bed superheater) because of reduced

temperature differential across the evaporator metal. Although stack loss is reduced and steam generation is proportionately increased, thermohydraulic nonlinearities cause steam flow to increase six times as much as the heat transfer rate, and the throttle steam temperature decreases.

Three of the varied parameters in Table 3 are the effective heat transfer areas of the evaporator, the primary superheater, and the secondary superheater. Each was varied by 1% to simulate the effects of manipulating heat transfer surfaces for purpose of boiler control.

4.1.2 Effective Evaporator Heat Transfer Surface

The reduction in evaporator surface represents the removal of 1% of the evaporator heat transfer area from the high heat transfer rate regime. The resulting decrease of heat transfer to the evaporator is small, being only 0.0122% compared with the 1% decrease in active surface. This is the result of a strong feedback reaction from the large evaporator heat transfer coefficient; reduction of heat to the evaporator causes drum pressure and temperature to drop, which in turn increases the temperature differential across the boiler metal and tends to restore heat transfer. The principal change in heat generation effected by reduction of active evaporator surface actually occurs in the bed superheater. Reduced drum pressure raises the evaporator steam enthalpy and necessitates lower steam flow to remove the nearly unchanged evaporator heat input; reduced steam flow through the secondary superheater then lowers its heat transfer by 0.8%.

Since heat transfer area and transfer coefficient appear as a product in the equations, these results may also be interpreted as a sensitivity analysis of the effect on system variables of a 1% uncertainty in the bed heat transfer coefficient K_b. This applies as well to the discussions of the primary and secondary superheater surfaces.

4.1.3 Primary Superheater Transfer Surface

Effective reduction of the primary superheater surface, as by dampering action, causes a much larger response than the corresponding change in the evaporator. A 1% reduction produces a 0.42% decrease in heat transfer. Table 3 shows that heat transfer in the evaporator is nearly independent of this change in the superheater; there is only a 0.02% decrease. On the other hand, half of the heat no longer absorbed in the primary superheater is recovered in the bed superheater, which is downstream in the steam path. Most of the remainder is lost through the stack.

4.1.4 Secondary (Bed) Superheater Transfer Surface

A similar pattern occurs in the case of a 1% reduction in the secondary superheater surface. Heat transfer in the evaporator is nearly unchanged (-0.0046%). The primary superheater, downstream in the gas path, picks up most of the heat no longer absorbed in the bed superheater.

In short, changes in the evaporator are seen to have a strong effect on the superheater, while changes in the superheaters have a comparatively minor effect on the evaporator. This is because both superheaters are downstream of the evaporator in the steam path, and disturbance signals generated in the evaporator propagate directly to the superheaters. On the other hand, with the evaporator upstream of the superheaters, disturbance signals in these units reach the evaporator only indirectly through the condenser and feedwater loop and are largely damped out by high heat capacitances and impedances along that path.

The observed interaction between the superheaters in which the output of one tends to increase when the other decreases may be more characteristic of fluid-bed boilers than of some conventional boilers. Because of the locations of the secondary superheater in the bed, the superheaters are each downstream of the other in one fluid path or the

other. The primary superheater is downstream of the secondary superheater in the gas path, and the secondary superheater is downstream of the primary superheater in the steam path. Thus, direct coupling occurs between them regardless of which one is disturbed.

The data for fluidizing air flow (third from last column in Table 3) show it to be insensitive to the steam side disturbances investigated. This is because air flow is regulated primarily by the ID and FD fans. Steam flow does not show an analogous insensitivity to gas side disturbances.

4.2 INFLUENCE OF FEEDWATER HEATING ON DYNAMICS

The model was used to estimate certain effects of feedwater heating. Steam was extracted from the condenser at a point where the enthalpy and pressure were a fraction e_t of throttle steam conditions. The numerical value of e_t was set at 0.9, corresponding to high-pressure extraction. The system was disturbed by a 1% reduction in firing rate. Table 4 shows the change in equilibrium values of selected variables, with and without feedwater heating. The data are in pairs, as in the previous table; the upper number of each pair is the change in units at the head of the column; the lower number of a pair is the percentage change.

Feedwater heating appears to benefit plant dynamics by reducing the magnitude of change in most of the listed variables by approximately a factor of 2. The change in bed temperature, important in SO_2 removal efficiency among other things, was reduced in magnitude by more than a factor of 3, from $\Delta T_b = 4.3°F$ to $\Delta T_b = 1.3°F$. The stabilizing effect of feedwater heating is the consequence of having part of the firing-rate-induced disturbance in steam flow fed directly back to the evaporator and superheaters without attenuation through the condenser circuit.

Table 4. Some effects of adding feedwater heating.
Changes resulting from 1% reduction in firing rate

Plant design	Evap. power (MW)	Prim. SH power (MW)	Sec. SH power (MW)	Bed temp. (°F)	Prim. SH metal temp. (°F)	Sec. SH metal temp. (°F)	Drum temp. (°F)	Throttle steam temp. (°F)	Throttle steam press. (psig)	Throttle steam flow (lb/s)
Without FWH[a]	0.11	-0.0004	-0.3	4.3	3.9	28	-6.9	28	-114	-1.1
	1.2	-0.12	-6.7	0.28	0.47	2.4	-1.0	2.8	-4.4	-6.3
With FWH	0.084	-0.0014	-0.2	-1.3	1.3	13.5	-4.1	14	-69	-0.65
	0.98	-0.43	-4.3	-0.08	0.16	1.1	-0.59	1.4	-2.6	-3.7

[a]Change (upper datum) and percent change (lower datum) in state variable; FWH = Feedwater heater.

5. PLANT CONTROL

5.1 CONTROLLER DESIGN

A streamlined control system of the load-following type was added to the model (Fig. 4). With slight modification, the direct-energy-balance or boiler-following type can be simulated. In keeping with the objective of developing a basic model, only major control loops are explicitly treated.

Principal loops include control of the following:

1. Firing rate. Boiler demand (target load) is determined from the superheater outlet steam flow and throttle pressure error. Boiler demand is compared with fuel flow, and firing rate is adjusted to eliminate throttle-pressure error.

2. Secondary (and primary) air. At a given excess air setpoint, boiler demand determines the needed air flow. This is compared with the existing air, and the inlet damper is positioned to zero the flow error.

3. Induced draft. Furnace pressure is regulated by a two-element controller that combines pressure error and a feedforward signal from boiler demand as inputs to the outlet damper.

4. Steam temperature. Steam temperature error at the throttle provides the signal to position the attemperator valve. Additionally, throttle pressure error is used as a trim on the steam temperature setpoint to provide over- and underfiring as needed during load changes.

5. Throttle valve. Because the simulation replaces a steam turbine with a condenser that has somewhat different thermohydrodynamics, changes in the throttle valve setting will not necessarily produce the same responses as in a utility plant. For purposes of load-following simulations it is desirable to choose a throttle valve control mode that mimics the behavior in a utility plant in important ways. With the scheme used in the model, the throttle valve is manipulated to maintain the condenser outlet water temperature

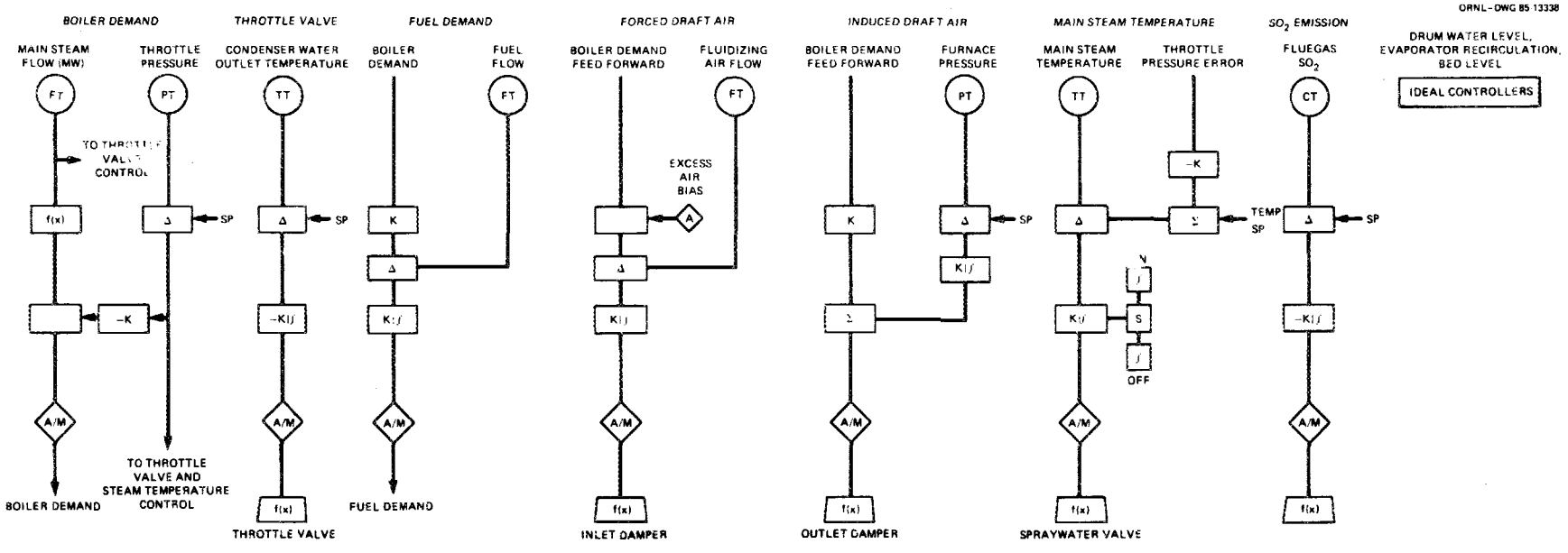

Fig. 4. Control system.

at setpoint. This forces the load (condenser heat transfer) to be proportional to steam flow rate, a major characteristic of turbines. Without this action, the condenser outlet temperature varies with flow, and load is not proportional to flow. The model allows variation of condenser air flow to represent load change.

6. SO_2 emission. The controller operates on the flue gas SO_2 error signal, and the calcium-to-sulphur ratio (limestone feed rate) is varied to null the setpoint error. Dead time of the SO_2 detector is not explicitly represented in the present controller (i.e., boiler transients are assumed long compared with detector dead time).

Each of the controllers uses proportional plus reset (integral) action. As will be discussed later, the firing rate controller has an optional derivative term. Ideal controllers are used to maintain drum and bed levels and recirculation.

5.2 CONTROLLER TUNING

The control system was tuned to full-power conditions. Controller settings are summarized in Table 5. Using a tuning procedure similar to the ultimate sensitivity method, a 5% step reduction in setpoint was

Table 5. Controller settings

Control loop	Proportional (gain)	Integral (repeats/min)	Derivative (min)
Throttle valve	1.9	0.6	0
Fuel demand	1.0	0.3	1.7
Excess air	18	0.6	0
Furnace pressure (draft)	19	0.6	0
Throttle steam temperature	100	0.6	0
SO_2	26	0.6	0

made to force the system variables to oscillate. Proportional gain settings were established such that the amplitude damping ratios were near 0.25, corresponding to the theoretical minimum area (product of setpoint error and time) under the recovery curves. This is illustrated in Fig. 5 for throttle steam pressure, the master signal for the control system. A 5% reduction in load was made, and the desired amplitude ratio was achieved with a gain setting of 1. For comparison, Fig. 6 shows the pressure oscillation with the gain increased twofold. Oscillation is divergent, and, of course, control is lost.

While the proper gain was being determined in Fig. 5, reset was temporarily turned off. When a transient calculation is terminated, the model automatically calculates the final equilibrium values with full controls (including reset) and presents these data as the last points on plotted curves. The resulting vertical tail on the pressure curve in Fig. 5 indicates the setpoint error (about 30 psi) that would result without reset. Figure 7 shows the same run with reset turned on at 0.3 repeats/min. Setpoint error (tail of curve) is vanishing, as desired.

5.3 TIME DELAYS IN A FLUID-BED PLANT

Heat capacities delay the propagation of temperature signals through the plant, and these time lags are a major problem in control design. Table 6 shows principal heat capacities of the simulated plant. The bed limestone mass is the largest single contributor, about 40% of the total. This capacity causes a lag between any change of firing rate and the resulting variation of steam pressure that provides the feedback signal for coal feed control. An estimate of the lag may be calculated from the equivalent resistance-capacitance (RC) time constant of the bed heat transfer coefficient and heat capacity, using the formula,

$$t_{lag} \sim 1/RC = M_b c_b / A_b h_b \quad ,$$

where M_b and c_b are respectively the bed mass and specific heat, and A_b and h_b are the heat transfer area and transfer coefficient. For the

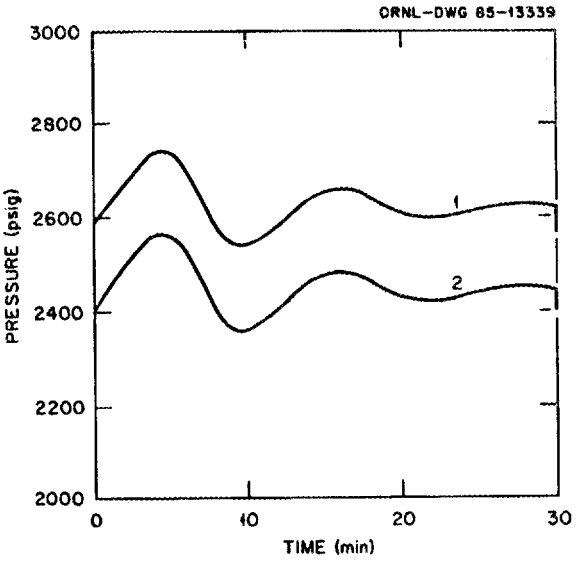

Fig. 5. Controlled response of drum (1) and throttle (2) pressures to 5% step reduction in load. No reset in coal-feed loop.

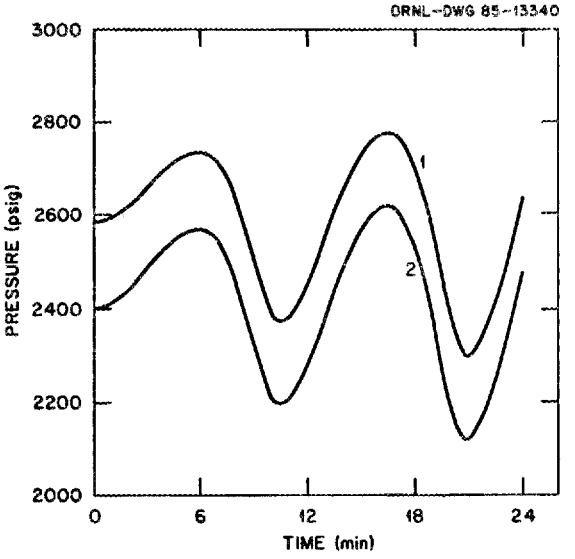

Fig. 6. Divergent pressure response with gain increased twofold. Drum (1), throttle (2).

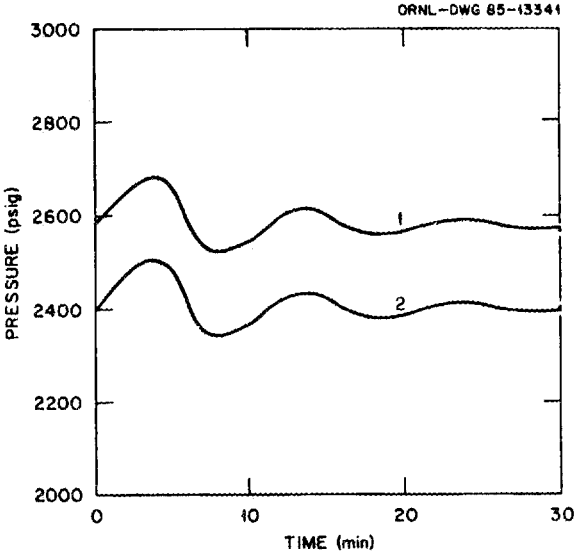

Fig. 7. Controlled response of drum (1) and throttle (2) pressures to 5% step change in load with reset in coal-feed loop.

Table 6. Principal system heat capacities expressed in full power minutes of stored heat

Boiler (metal and water)	3
Primary SH	2
Secondary SH	0.5
Preheater	1.5
Bed	6
Condenser	2
Total	15

simulated plant, t_{lag} ~ 2-3 min. This particular lag is unique to fluidized-bed boilers, and its impact on plant control needs to be studied.

The effects of bed capacity were analyzed in part by the reaction curve method in which the control loop for fuel demand was opened and a step reduction of 1% was made "manually" in coal feed. Curve 1 in Fig. 8 shows the resulting decrease in steam pressure as a function of time. The overall shape of the curve is sigmoidal, characteristic of a second-order lag (Fig. 8 insert), and the section of particular interest is that from time zero out to the point of inflection, shown in the figure. Extrapolation of the inflection-point slope back to the initial pressure line is a standard measure of the time lag (2.7 min here) between change of coal feed and steam pressure response. This value includes all heat capacities and transport delays associated with the steam circuit and coal feed. To determine the part associated specifically with bed mass, the calculation was repeated with the limestone mass mathematically reduced to one-fifth full value (zero value would cause the computer to divide by zero). Curve 2 resulted. The difference between the lag times of curves 1 and 2, adjusted to total bed mass, gives 1.9 min as the lag associated with the bed heat

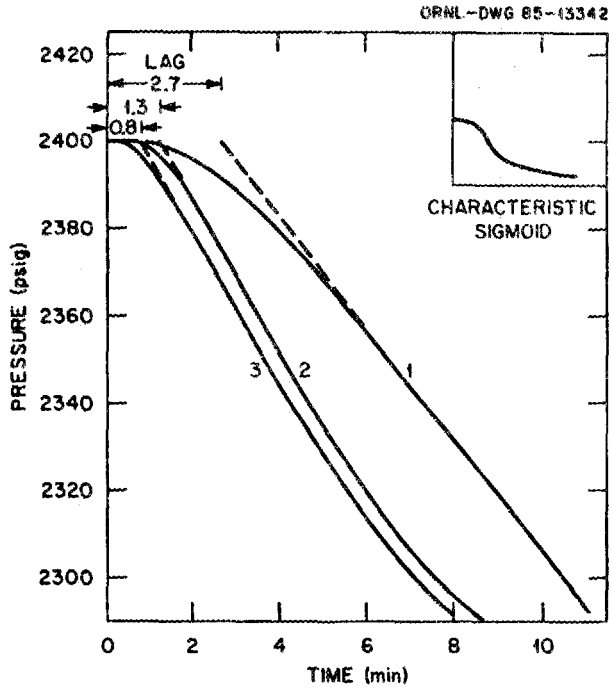

Fig. 8. Reaction curve analysis of system time lags. Total lag (1), lag with reduced bed mass (2), lag with reduced bed mass and reduced coal transport and burnup times (3).

capacity. Such lags commonly reduce the maximum stable gain settings. Since speed of response tends to decline with reduced gain, lags can limit automatic control, as, for example, in following rapid load changes. Whether bed lag is limiting here requires further analysis, since other factors contribute to the proper gain setting.

The reaction-curve optimum gain setting is computed from the formula

$$G \propto 1/LS \quad ,$$

where L is lag and S is inflection-point slope (rate of change). The optimum, therefore, depends on rate of response S as well as time of

response L. Gains calculated from this index are 1.48 from curve 1 with full bed mass and 1.51 from curve 2 with one-fifth bed mass. Thus, within the accuracy of the method, the optimum is largely insensitive to the lag associated with bed mass. Physically this means that the bed heat capacity not only delays temperature signals to the steam but also acts as a ballast or filter that attenuates them. While lags necessitate reduced gain, filtering requires increased gain to maintain suitable control, and the two bed effects tend to cancel. Such an insensitivity of gain setting to bed mass could be particularly significant in situations where bed level (mass) is varied for load following; the controller would tend to remain tuned irrespective of bed level.

Two important delays associated with the fuel are its transport time to the furnace and the burnup time constant of crushed coal particles. These delays may impact control somewhat differently than the bed delay. To show this, both coal delays were reduced from full value (15 s each in curve 2, Fig. 8) to one-fifth value (curve 3). The difference in lag between curves 2 and 3 is the expected 0.5 min sum of the two. The remaining 0.8 min delay of curve 3 is the sum of all other capacitance delays in the steam/water circuit (e.g., in the boiler metal and water).

In the case of the bed delay, curves 1 and 2 have different slopes such that the shorter delay of a smaller bed mass was compensated by increased response rate (slope), and the controller gain setting, inversely proportional to the product, remained essentially independent of bed mass. For the coal delays, however, curve 3 with reduced delay has the same slope as curve 2 with full delay; the optimum gain is therefore reduced by the ratio of the lags (about 50%). Typical of coal-fired plants, the AFBC's rate of automatic response to load change may be restricted by delays in coal transport and burnup (among other things).

Derivative control action may add compensating phase lead to these lags. Though frequently not included in conventional controls, the

derivative mode may be appropriate in a fluidized-bed plant to boost its rate of response. The solid curve in Fig. 9 shows the damped pressure response with optimum gain, reset, and derivative. With the derivative mode then turned off (dashed curve), the same gain is too high, and the oscillation is divergent. The stabilizing phase lead (the time difference between neighboring peaks of the two curves) is about 1 min. In this case, the derivative allows approximately 50% more gain and an increased rate of load change in autocontrol.

5.4 LOAD FOLLOWING

The model was used to investigate the rate and magnitude of load variation that the plant can be expected to follow and to determine the effects of certain operational strategies on load-following capability. Two types of load change were considered: abrupt, step-like change, and smoother, ramp change.

5.4.1 Abrupt Change

Starting at full power, a 5% step reduction was made in cooling air flow (load) at the condenser. The control system operated to maintain setpoints. Figures 10a through 10e show plant response. Most variables are held within nominal control range. Bed temperature (Fig. 10a, upper curve) experiences an initial drop of about 50°F with recovery in 8 min. Main steam temperature (Fig. 10a, lower curve) remains near setpoint. Sulphur capture (Fig. 10b) is closely controlled by modest variation of limestone feed (Fig. 10c).

The limiting variation is steam pressure. Main steam (Fig. 10d, lower curve) experiences an initial overshoot of about 115 psi. That the controller is having difficulty in holding steam pressure is evident from the swing in coal supply (Fig. 10e). The steam-pressure controller is tuned to full-power conditions and has the highest stable proportional gain setting as well as maximum derivative action to

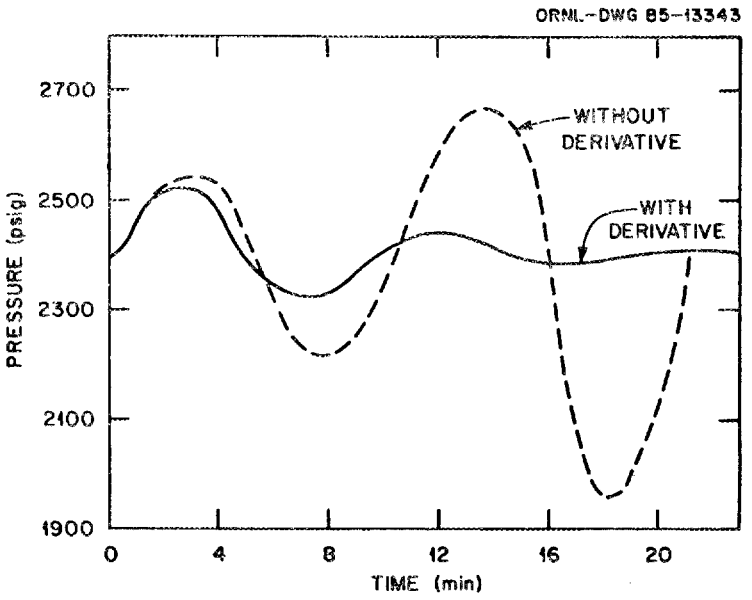

Fig. 9. Effect of adding derivative action to coal-feed control.

compensate RC and transport lags. In short, the controller is being driven as hard as it can be. These results suggest, therefore, that if steam pressure is to be held to within a few percentage points (commonly about 2%) of setpoint, sharp changes in load will be limited to approximately 5% magnitude.

5.4.2 Ramp Change

In practice, load changes are typically rather smooth ramps of varying steepness and duration. The next series of calculations considers how fast a ramp the plant can be expected to follow with the present controllers. Operational strategy is a major factor in this determination, and two possible strategies will be examined. For reasons discussed later, it will emerge that a key factor in load-following capability will be the extent to which the distributed

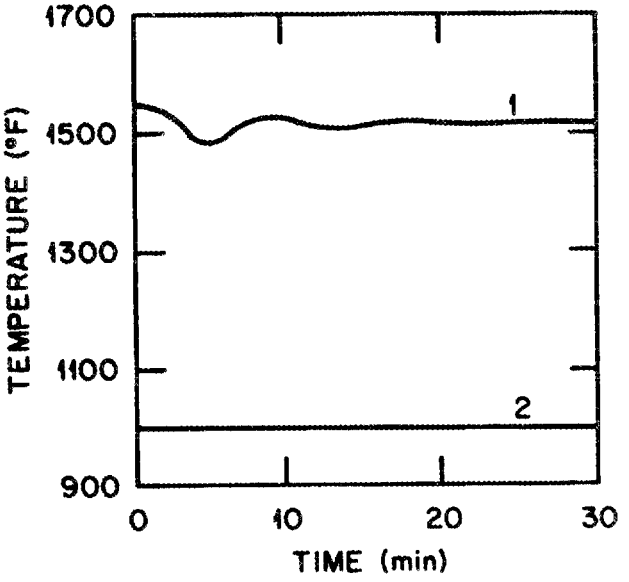

Fig. 10a. Effect on system variables of 5% step reduction in load. Temperature: bed (1), throttle (2).

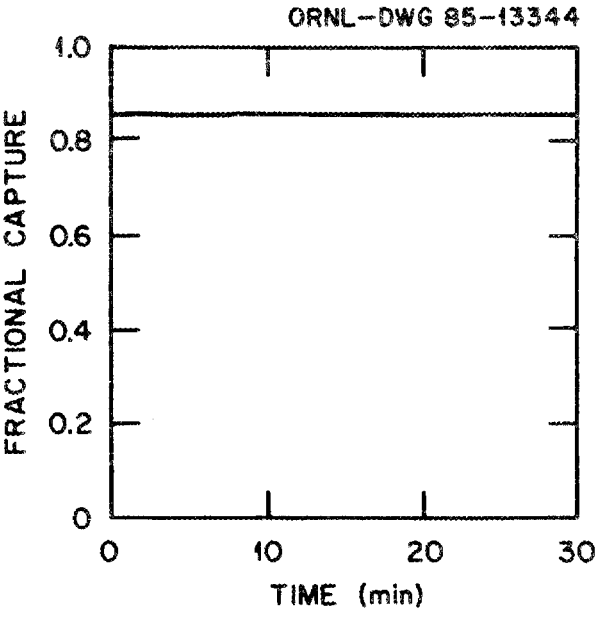

Fig. 10b. SO_2 capture.

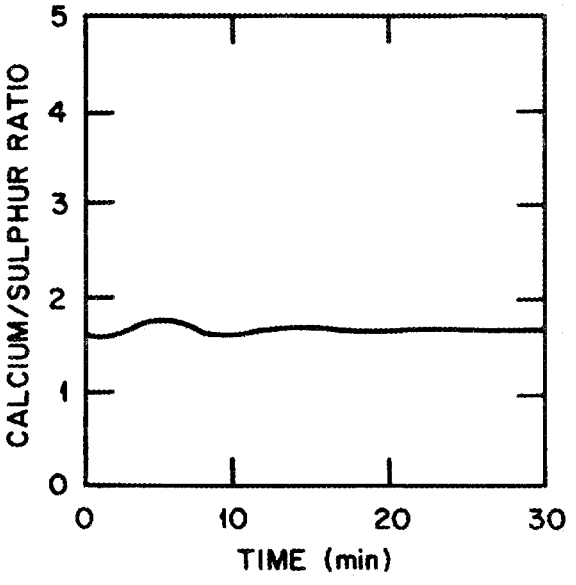

Fig. 10c. Limestone feed.

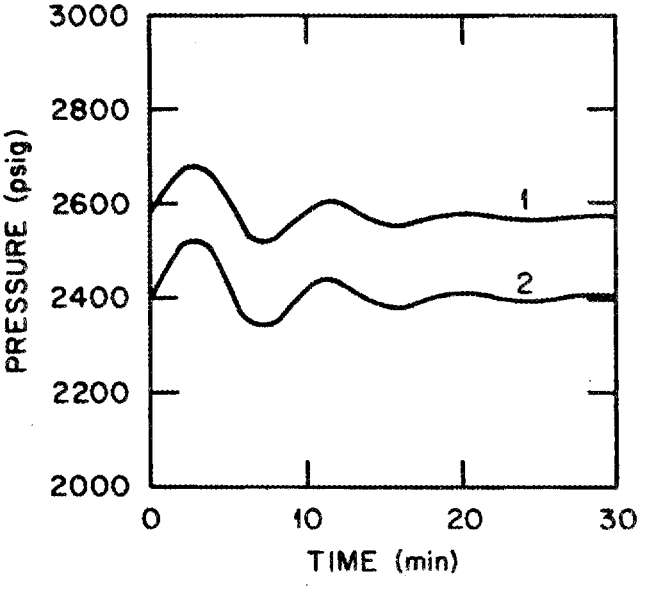

Fig. 10d. Steam pressure. Drum (1), throttle (2).

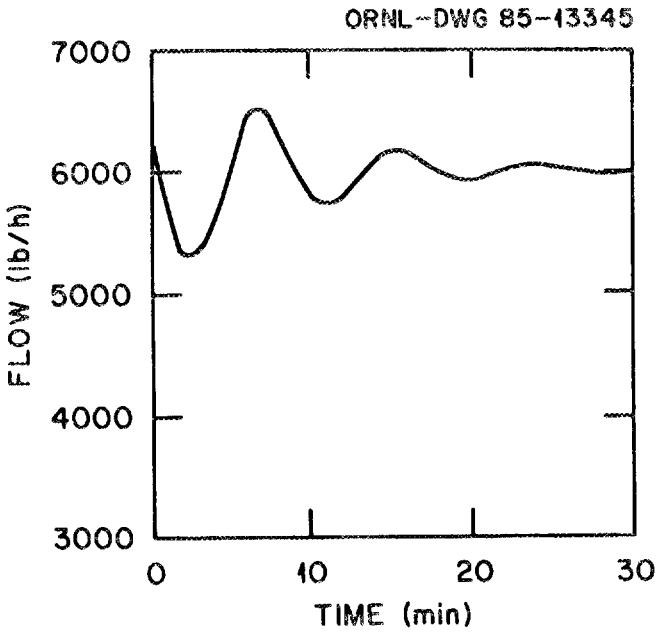

Fig. 10e. Coal feed.

(position dependent) ratio of fuel feed (heat supply) to operating heat transfer surface (heat sink) can be held constant across the bed.

A proposed mode of operation of AFBC plants calls for heat transfer surface to be removed from service for load-following purposes by shutting down (slumping) bed compartments. If a compartment's fraction of total heat generation is, for example, one-fourth, the load and coal feed will first be decreased by this amount, and then a compartment will be removed from service. Thus, fuel reduction and removal of heat transfer surface occur sequentially.

This sequential strategy was investigated by a simulation in which load was reduced by 25% over an interval of 33 min (a ramp of 0.75%/min), and then a compartment representing 25% of the bed was shut down. The model allows boiler and superheater surface to be removed in any proportion; in these studies, the same fraction (0.25) of each was removed.

The ramped reduction in condenser cooling (load demand) is shown in Fig. 11a. Mainsteam flow, power generation, coal feed, and superficial velocity (Figs. 11b through 11e) smoothly follow demand down to 75% load. The initial pressure overshoot (Fig. 11f) is 55 psi. Bed temperature (Fig. 11g) declines almost 200°F because nonlinear changes in steam flow and heat transfer coefficients cause a 5% increase in the proportion of generated heat that is removed in the bed versus the above-bed superheater. In this, the plant exhibits the tendency of shifting heat transfer that often occurs in boilers with superheaters.

The strongly temperature sensitive SO_2 capture experiences a decline from 85% to 70% removal (Fig. 11h) as a result of the suboptimal bed temperature. To maintain this level of SO_2 removal, the SO_2 controller increases limestone feed to a peak Ca/S ratio of 9 (Fig. 11i). Limestone feed at the peak is 15% greater than coal feed and for all practical purposes is probably near the limit of the control range.

Various control valve settings are shown in Fig. 11j. Thirty minutes into the transient, steam temperature control by spray-water regulation goes marginally out of the control range for a short time. To prevent integral windup, the controller automatically freezes reset action until the temperature returns to control range.

At 33 min, when the demand levels off at 75% of full load, a shutdown of one-quarter of the bed is effected. Removal of bed heat transfer surface from operation is made to occur by compartment slumping over a period of 25 min (Fig. 11k). Even at this average effective removal rate of only 1%/min, the slumping action causes the steam pressure (Fig. 11f) to nosedive below setpoint by about 120 psi. Thereafter, the system oscillates one or two cycles, and setpoints are restored about 30 min after slumping is initiated. During the initial load decrease, when coal feed is reduced, the ratio of fuel supply to heat transfer area (denoted the fuel-to-surface ratio) is lowered. Because of bed circulation, the lower ratio occurs more or less uniformly across the bed. Then, when a compartment is shut down, the original ratio is restored in the portion of the bed still in operation. This fluctuation in the fuel-to-surface ratio distribution, coupled with

ORNL-DWG 85-13346

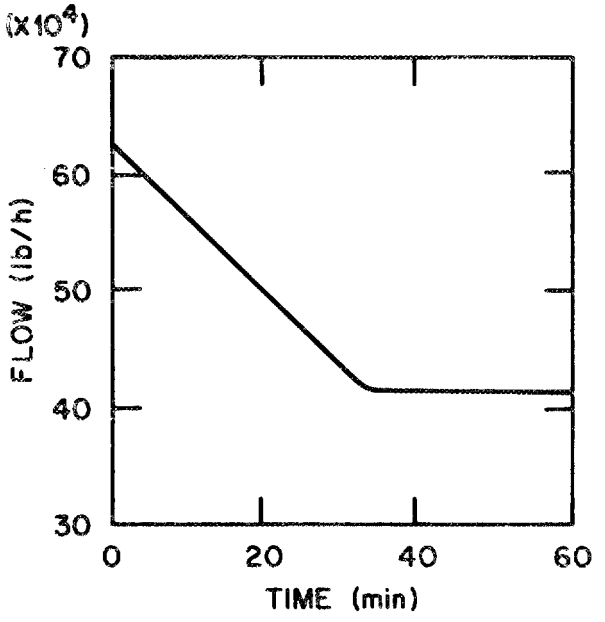

Fig. 11a. Effect on system variables of 25% runback of load at rate of 0.75%/min, with bed slumping after runback. Condenser cooling air (load).

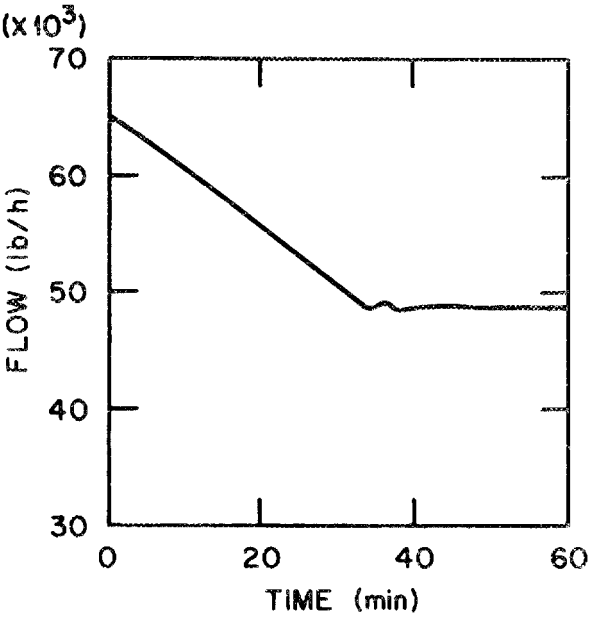

Fig. 11b. Main steam flow.

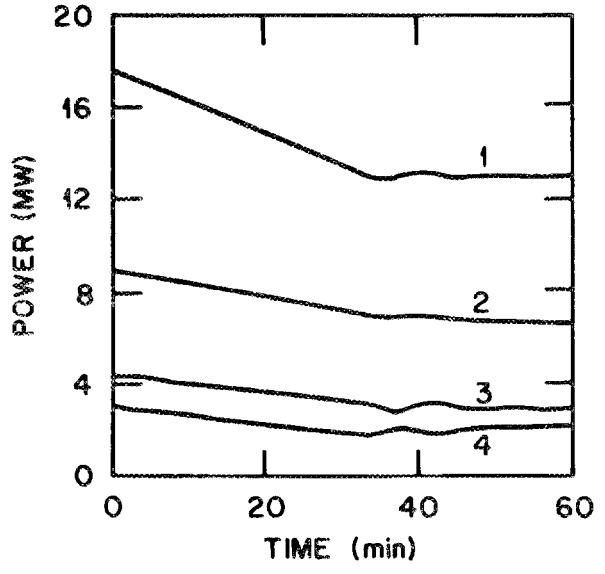

Fig. 11c. Power generation. Total power (1), evaporator (2), bed superheater (3), primary superheater (4).

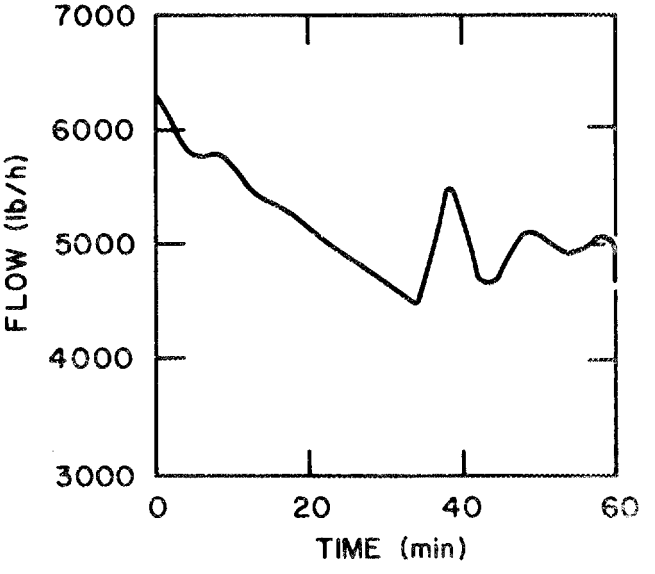

Fig. 11d. Coal feed.

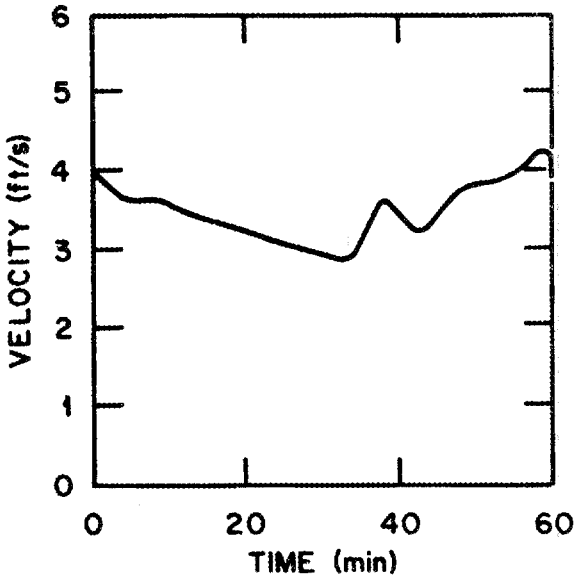

Fig. 11e. Superficial velocity.

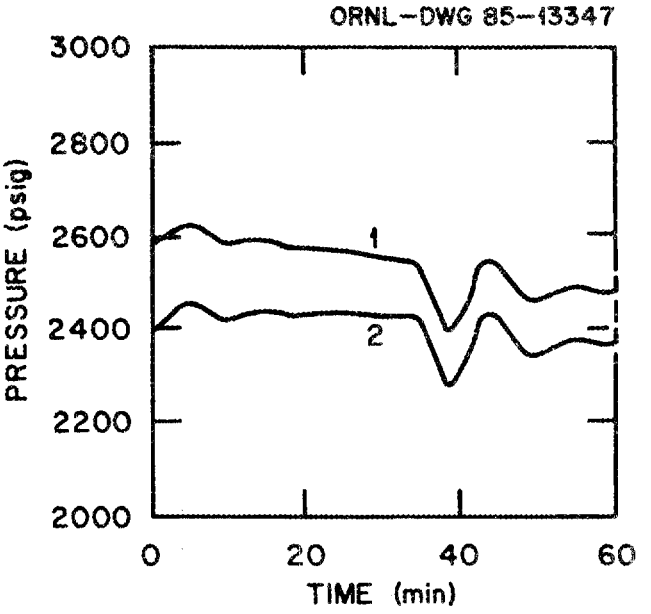

Fig. 11f. Steam pressure. Drum (1), throttle (2).

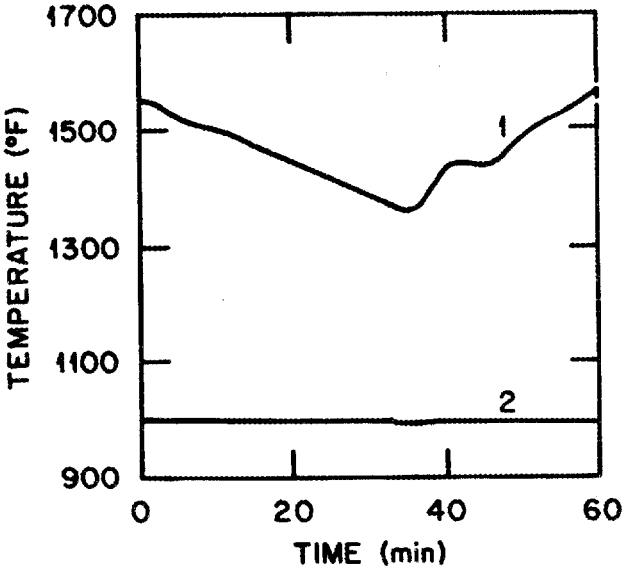

Fig. 11g. Temperature. bed (1), throttle (2).

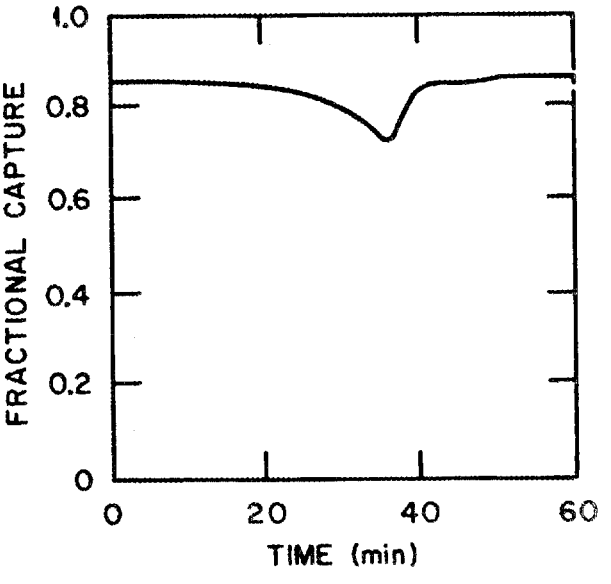

Fig. 11h. SO_2 capture.

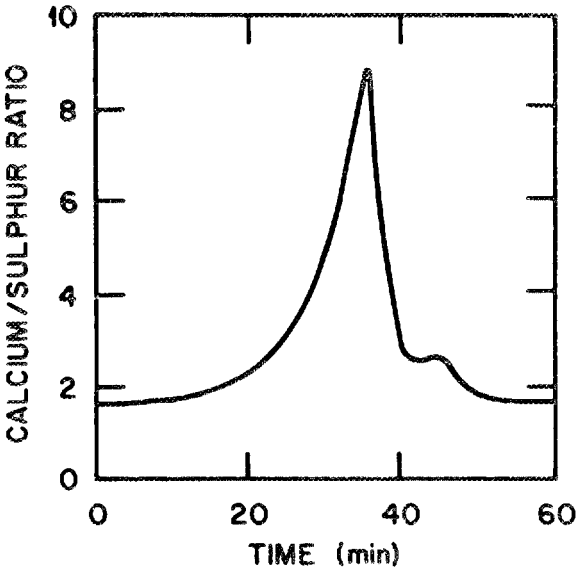

Fig. 11i. Limestone feed.

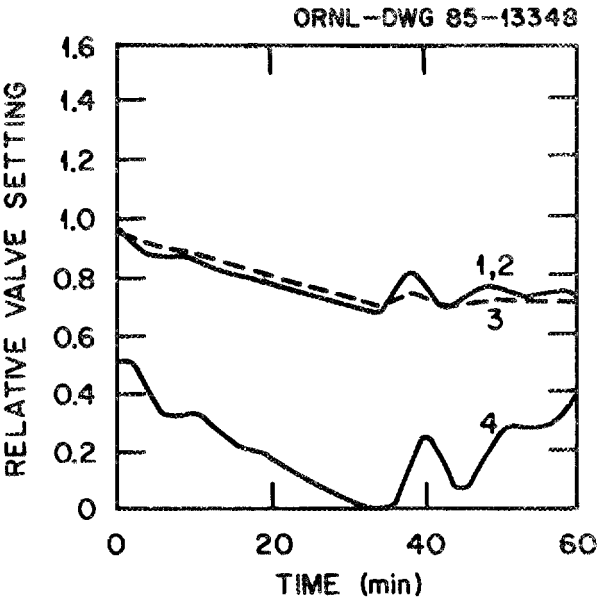

Fig. 11j. Control valve settings. FD damper (1), ID damper (2), throttle (3), spraywater (4).

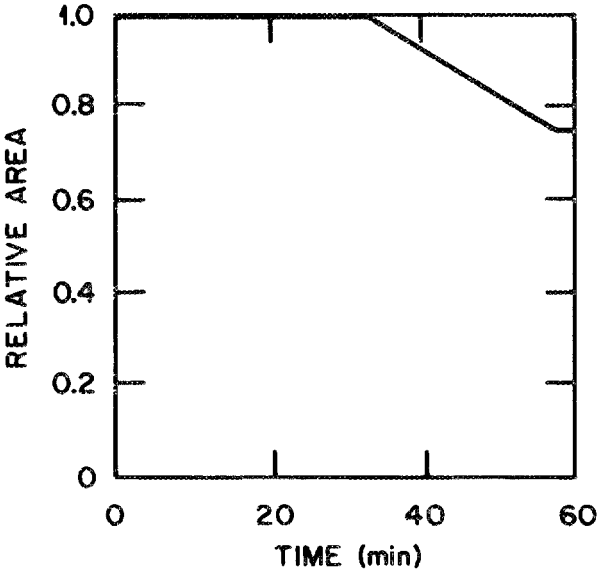

Fig. 11k. Fraction of bed fluidized and heat transfer surface active.

substantial heat capacities of the bed and pressure parts, upsets the temperature distribution. The magnitude of the ensuing disturbance is a function of the rate of both the load variation and the compartment shutdown operation. Apart from any other restrictions, these results indicate that automatic load following by sequential manipulation of coal feed and heat transfer surface will be limited to sustained ramps of less than about 1%/min.

An improved mode of operation is to vary coal feed and heat transfer surface simultaneously, such that their ratio remains continuously fixed throughout the bed. Two possible ways may be cited. First, since material circulation is a function of void fraction, which in turn is a function of superficial velocity, modulation of compartment air velocity may possibly provide the basis for regulation of coal infiltration and thereby the effective amount of heat transfer surface.

A second method of maintaining a balanced fuel-to-surface distribution is by continuous variation of the fluidized-bed mass and height to expose surface as necessary. In a comparative study of this type of operation, the previous ramp (25% reduction in load at 0.75%/min) was repeated, and the same state variables are shown in Figs. 12a through 12k. The improvement in control is evident. Most variables remain so close to setpoint that the deviation can't be read from the curves. Pressure (Fig. 12f) varies less than 20 psi, and bed temperature (Fig. 12g) changes only 11°F. Sulphur removal (Fig. 12h) remains virtually at setpoint. In contrast with the previous spiked limestone feed, the calcium-to-sulphur ratio now remains at nominal value throughout load reduction (Fig. 12i). Simultaneous manipulation of coal feed and heat-transfer surface maintains a balanced distribution of heat production and removal across the bed and pressure parts and minimizes the temperature transients that disturbed the system under sequential operation.

In a conventional plant, boiler heat transfer coefficients are a function of gas velocity, and distribution of heat transfer may be controlled by smooth variation of gas velocity, dampers, and gas recirculation. In an AFBC, the bed heat transfer coefficient is largely

ORNL-DWG 85-13349

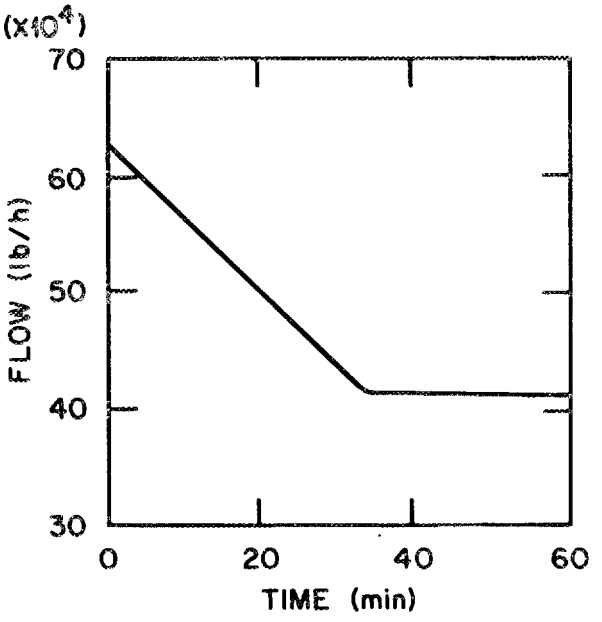

Fig. 12a. Effect on system variables of 25% runback of load at 0.75%/min, with variable bed height. Condenser cooling air (load).

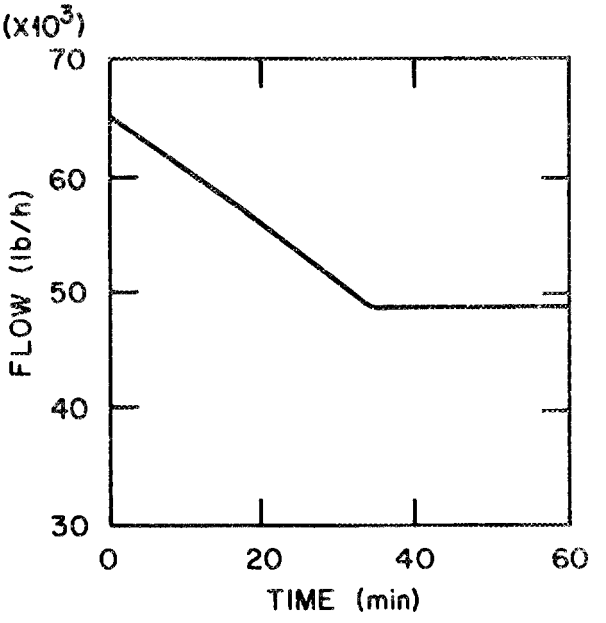

Fig. 12b. Main steam flow.

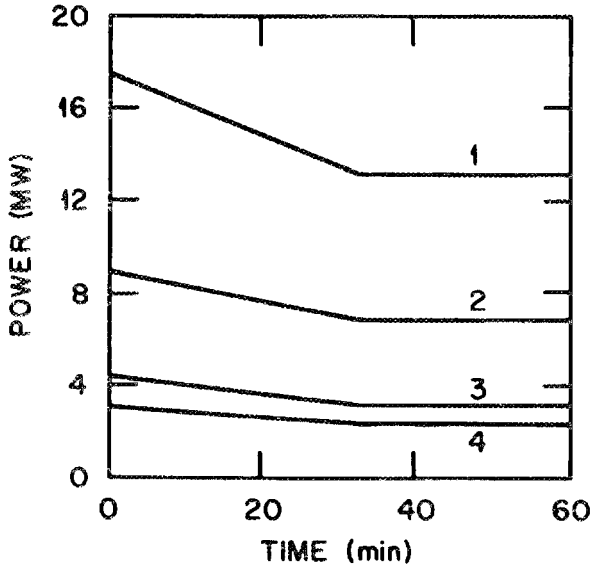

Fig. 12c. Power generation. Total power (1), evaporator (2), bed superheater (3), primary superheater (4).

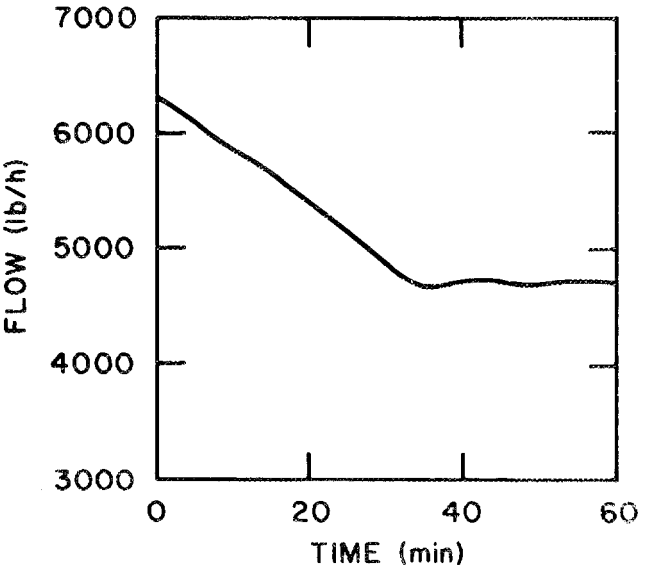

Fig. 12d. Coal feed.

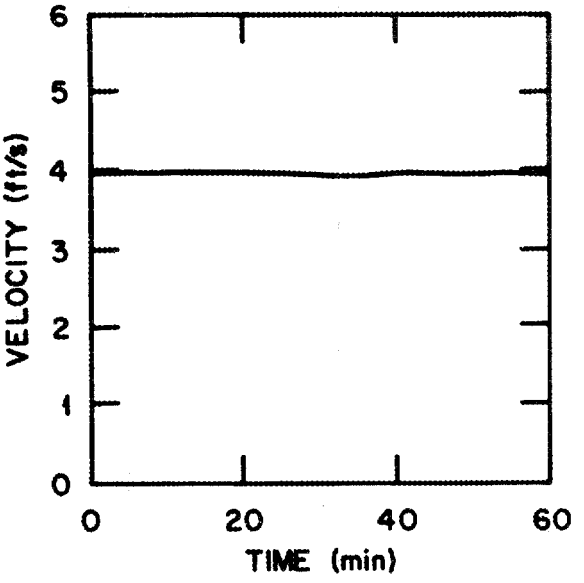

Fig. 12e. Superficial velocity.

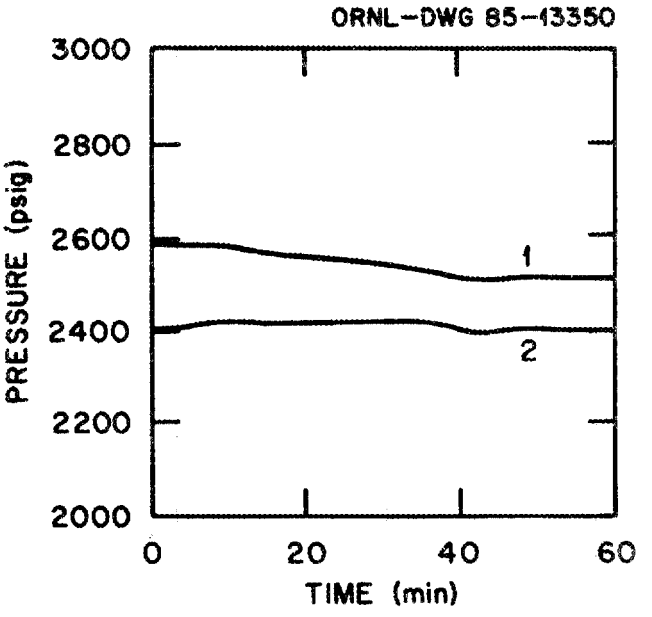

Fig. 12f. Steam pressure. Drum (1), throttle (2).

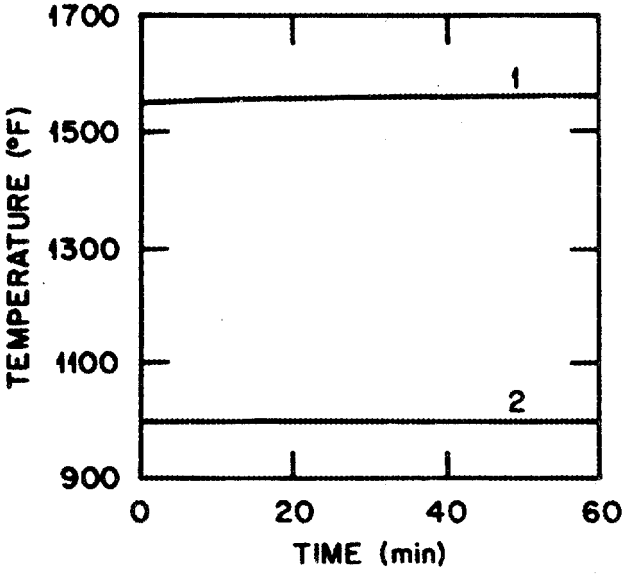

Fig. 12g. Temperature. bed (1), throttle (2).

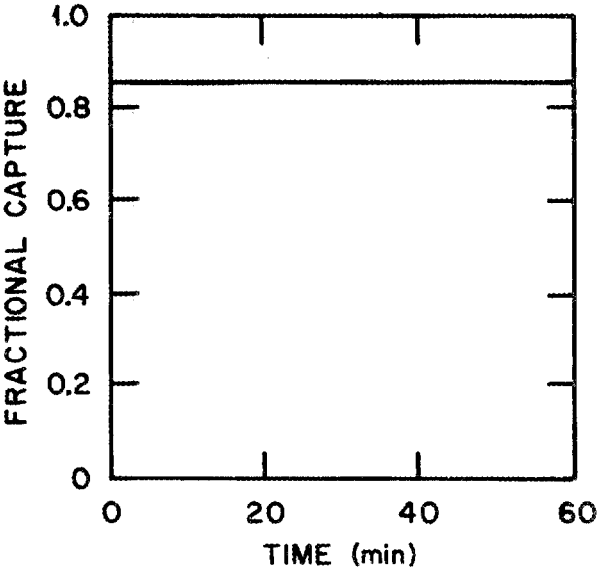

Fig. 12h. SO_2 capture.

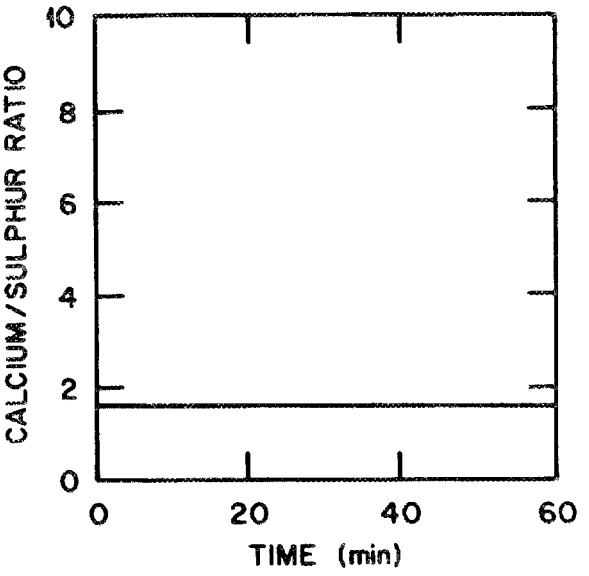

Fig. 12i. Limestone feed.

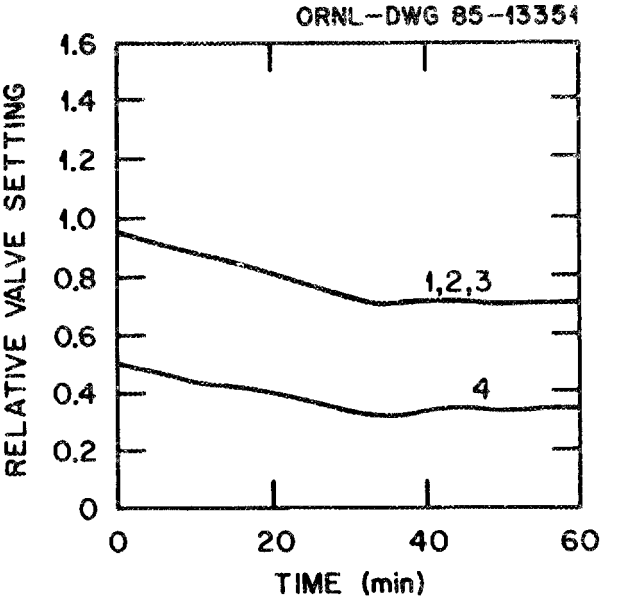

Fig. 12j. Control valve settings. Throttle (1), FD damper (2), ID damper (3), spraywater (4).

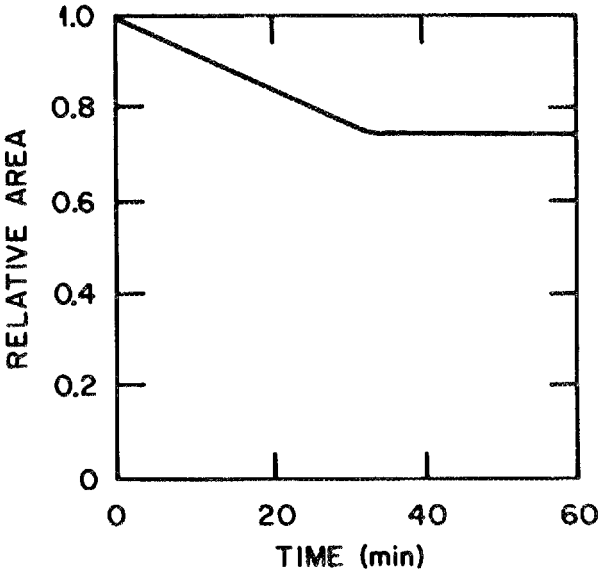

Fig. 12k. Fraction of bed fluidized and heat transfer surface active.

insensitive to gas velocity, and the slumping of compartments becomes a counterpart of dampering that may introduce disturbances not present in the conventional plant. Any procedure for continuously maintaining the desired heat distribution in the bed has the net effect of attempting to operate it, in this respect, more like a conventional plant.

A simulation was run to determine the maximum sustained ramp that the modeled AFBC can automatically follow with simultaneous manipulation of coal feed and heat transfer surface. Load was reduced 25% in 5 min. The results are shown in Figs. 13a through 13k. There is an initial pressure excursion of about 100 psi. Other variables remain well controlled. This simulation suggests that a properly operated fluidized-bed plant may be able to automatically follow ramps of up to about 5%/min, which is competitive with leading conventional and nuclear plants.

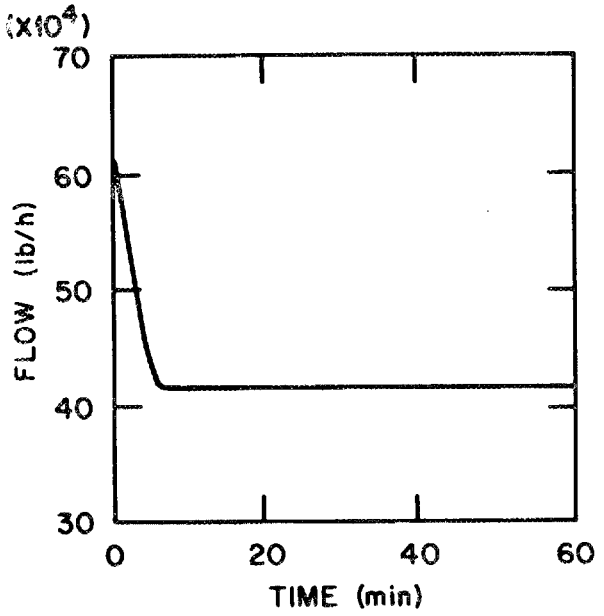

Fig. 13a. Maximum load-following capability (5%/min) using variable bed height. Condenser cooling air (load).

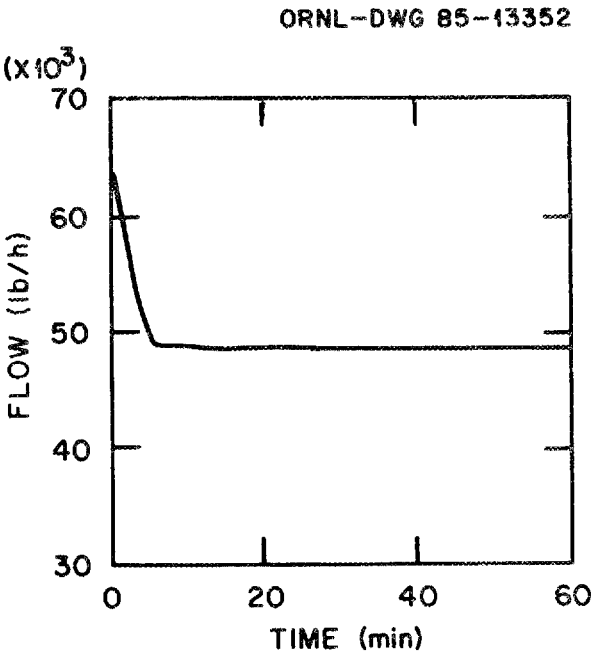

Fig. 13b. Main steam flow.

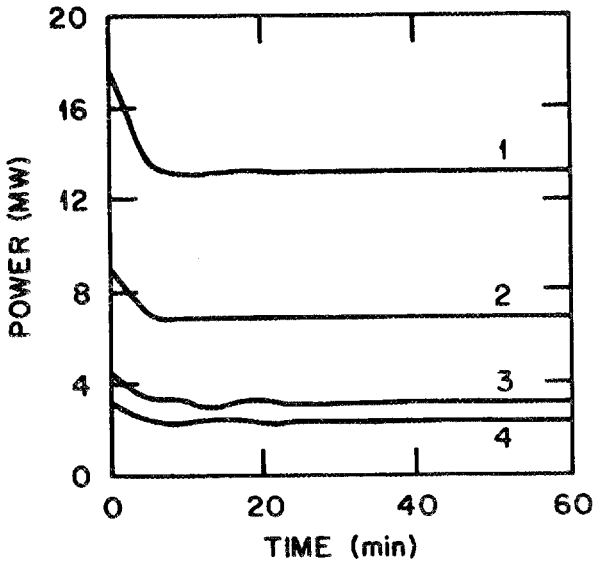

Fig. 13c. Power generation. Total power (1), evaporator (2), bed superheater (3), primary superheater (4).

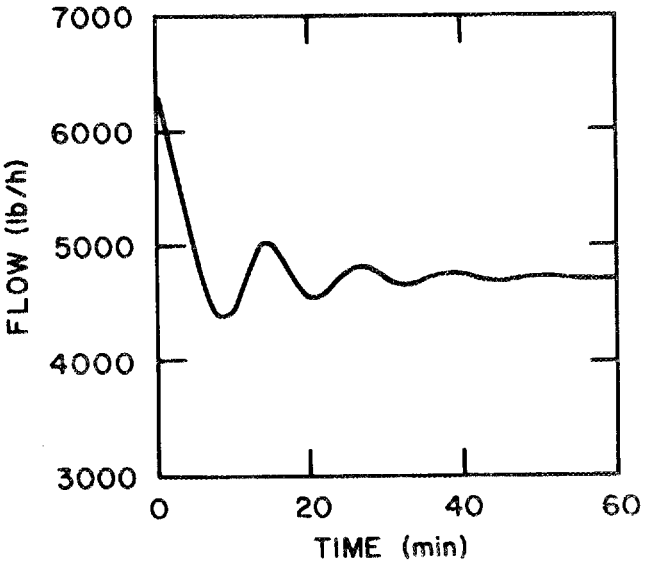

Fig. 13d. Coal feed.

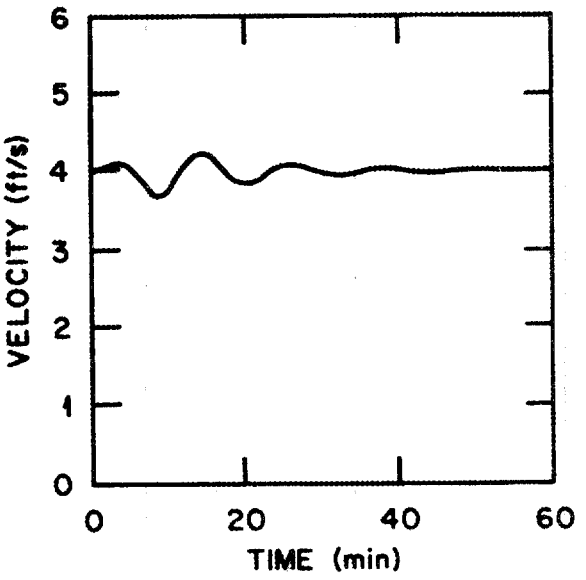

Fig. 13e. Superficial velocity.

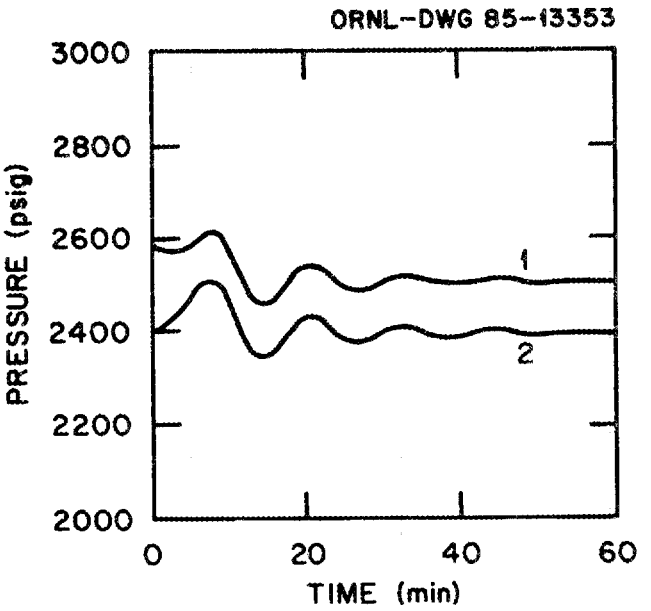

Fig. 13f. Steam pressure. Drum (1), throttle (2).

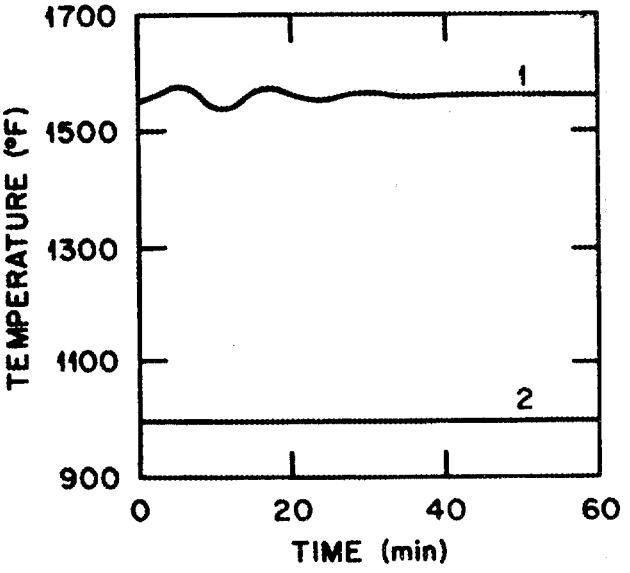

Fig. 13g. Temperature. Bed (1), throttle (2).

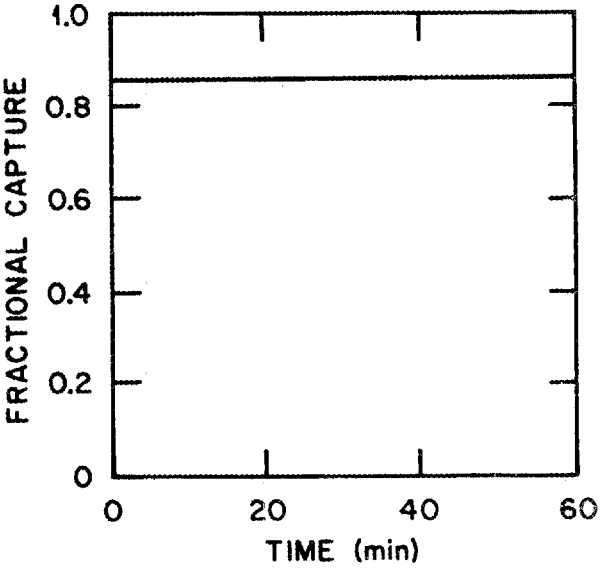

Fig. 13h. SO_2 capture.

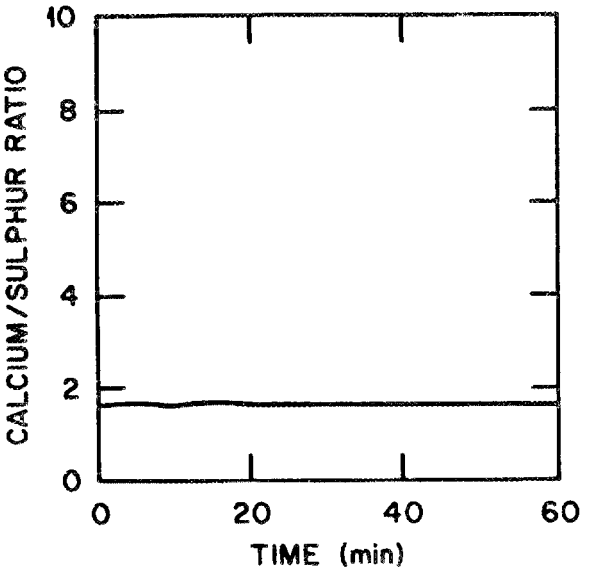

Fig. 13i. Limestone feed.

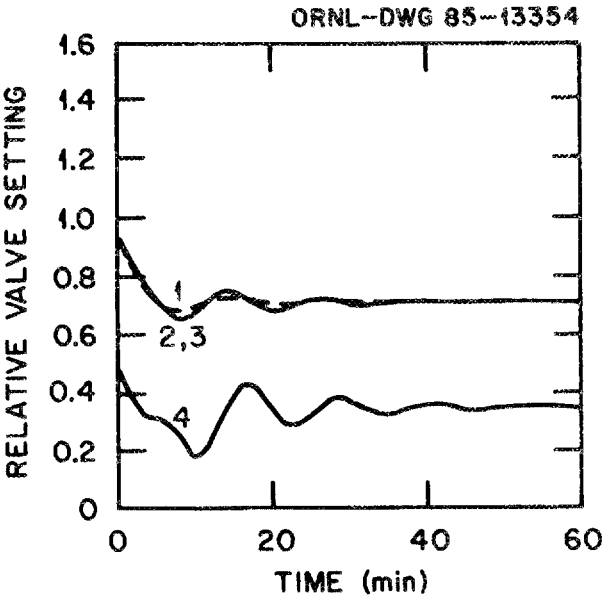

Fig. 13j. Control valve settings. Throttle (1), FD damper (2), ID damper (3), spraywater (4).

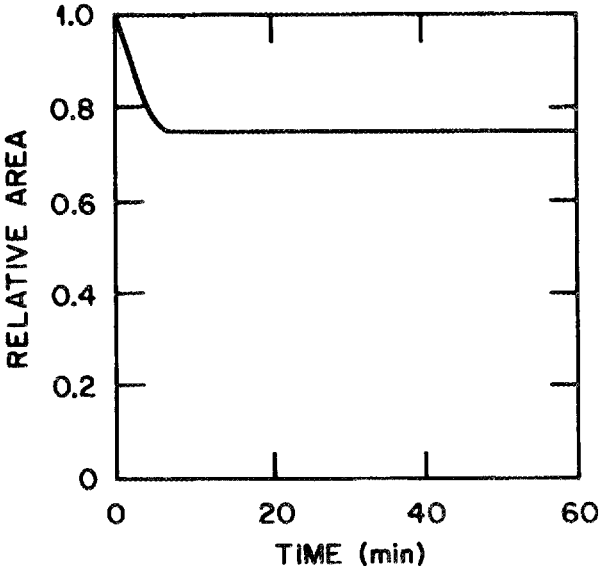

Fig. 13k. Fraction of bed fluidized and heat transfer surface active.

ACKNOWLEDGMENT

This work was funded in part by the Tennessee Valley Authority.

REFERENCES

1. A. Ray, D. A. Berkowitz, and V. Sumaria, "Mathematical Modeling and Digital Simulation of the MERC Component Test and Integration Unit," MTR-3447, May 1977.

2. J. R. S. Thom, W. M. Walker, T. A. Fallon, and G. F. S. Reising, "Boiling in Subcooled Water During Flow Up Heated Tubes or Annuli," Proc. Inst. Mech. Eng. 3C180:226 (1965-66).

3. Babcock and Wilcox, Steam/Its Generation and Use, 39th ed., 1978, pp. 4-10.

4. F. W. Dittus and L. M. K. Boelter, Univ. of Calif. Publ. Eng. 2:443 (1930).

5. J. P. Holman, Heat Transfer, 4th ed., McGraw-Hill, 1976, p. 180.

6. Babcock and Wilcox Company, Steam/Its Generation and Use, 39th ed., 1978, p. 6-2.

7. T. E. Dowdy et al., "Summary Evaluation of Atmospheric Pressure Fluidized Bed Combustion Applied to Electric Utility Large Steam Generators," EPRI FP-308, Vol. 2, Appendix 6. Electric Power Research Institute, Palo Alto, Calif., 1976.

8. R. P. Apa et al., "6- × 6-ft Atmospheric Fluidized-Bed Combustion Development Facility and Commercial Utility AFBC Design Assessment," EPRI CS-2930, Interim Report, Electric Power Research Institute, Palo Alto, Calif., March, 1983.

9. D. Merrick and J. Highley, AICHE Symposium Series 70, 137, 366-378 (1974).

APPENDIX

The following thermodynamic correlations were derived from standard steam tables for the simulated plant operating range, with throttle pressure of 2600 psig.

Superheated steam:

$$h_{s_1} = 2697 - 0.904ps_1 - 1.33Ts_1 + 9.6 \times 10^{-4} p_{s_1} T_{s_1} \quad (A.1)$$

$$h_{s_2} = 1109 - 0.132ps_2 + 0.437Ts_2 + 9.6 \times 10^{-5} ps_2 Ts_2 \quad (A.2)$$

$$p_a = -33.1 + 0.041h_a - 1008\rho_a + 1.21\rho_a h_a \quad (A.3)$$

$$h_a = 1263 - 0.231p_a + 0.279T_a + 1.98 \times 10^{-4} p_a T_a \quad (A.4)$$

Saturated steam and water:

$$T_d = 541.1 + 22.8\rho_s - 0.812\rho_s^2 \quad (A.5)$$

$$p_d = 434.4 + 363.5\rho_s - 12.3\rho_s^2 \quad (A.6)$$

$$h_s = 1242 - 21.1\rho_s + 0.174\rho_s^2 \quad (A.7)$$

$$u_s = 734 + 6.76\rho_s - 0.363\rho_s^2 \quad (A.8)$$

$$u_w = 512 + 24.9\rho_s - 0.755\rho_s^2 \quad (A.9)$$

$$\rho_w = 48.8 - 2.08\rho_s + 0.0322\rho_s^2 \quad (A.10)$$

$$h_w = 490 + 40.4\rho_s - 1.16\rho_s^2 \quad (A.11)$$

Subcooled water:

$$h_f = -110 + 1.2T_f \quad (A.12)$$

INTERNAL DISTRIBUTION

1. R. A. Bradley
2. B. G. Eads
3. D. N. Fry
4. F. R. Mynatt
5-9. O. L. Smith
10. R. S. Stone
11. R. S. Wiltshire
12. J. B. Ball (Advisor)
13. M. J. Kopp (Advisor)
14. P. F. McCrea (Advisor)
15. H. M. Paynter (Advisor)
16-17. Central Research Library
18. Y-12 Document Reference Section
19. I&C PIPC
20-21. Laboratory Records
22. Laboratory Records, ORNL RC
23. ORNL Patent Section

EXTERNAL DISTRIBUTION

24. Assistant Manager for Energy Research and Development, DOE-ORO, Oak Ridge, TN 37831
25. Manager, Office of Fossil Energy, DOE, Washington, DC 20545
26. Director, DOE Morgantown Energy Research Center, P.O. Box 800, Morgantown, WV 26506
27-56. Office of Scientific & Technical Information, Oak Ridge, TN 37831